



University Transportation Research Center - Region 2

Final Report

Potential Sites for Tidal Power in New Jersey

Performing Organization: The City College of New York, CUNY



May 2014

Sponsors:
New Jersey Department of Transportation (NJDOT)
University Transportation Research Center - Region 2

University Transportation Research Center - Region 2

The Region 2 University Transportation Research Center (UTRC) is one of ten original University Transportation Centers established in 1987 by the U.S. Congress. These Centers were established with the recognition that transportation plays a key role in the nation's economy and the quality of life of its citizens. University faculty members provide a critical link in resolving our national and regional transportation problems while training the professionals who address our transportation systems and their customers on a daily basis.

The UTRC was established in order to support research, education and the transfer of technology in the field of transportation. The theme of the Center is "Planning and Managing Regional Transportation Systems in a Changing World." Presently, under the direction of Dr. Camille Kamga, the UTRC represents USDOT Region II, including New York, New Jersey, Puerto Rico and the U.S. Virgin Islands. Functioning as a consortium of twelve major Universities throughout the region, UTRC is located at the CUNY Institute for Transportation Systems at The City College of New York, the lead institution of the consortium. The Center, through its consortium, an Agency-Industry Council and its Director and Staff, supports research, education, and technology transfer under its theme. UTRC's three main goals are:

Research

The research program objectives are (1) to develop a theme based transportation research program that is responsive to the needs of regional transportation organizations and stakeholders, and (2) to conduct that program in cooperation with the partners. The program includes both studies that are identified with research partners of projects targeted to the theme, and targeted, short-term projects. The program develops competitive proposals, which are evaluated to insure the most responsive UTRC team conducts the work. The research program is responsive to the UTRC theme: "Planning and Managing Regional Transportation Systems in a Changing World." The complex transportation system of transit and infrastructure, and the rapidly changing environment impacts the nation's largest city and metropolitan area. The New York/New Jersey Metropolitan has over 19 million people, 600,000 businesses and 9 million workers. The Region's intermodal and multimodal systems must serve all customers and stakeholders within the region and globally. Under the current grant, the new research projects and the ongoing research projects concentrate the program efforts on the categories of Transportation Systems Performance and Information Infrastructure to provide needed services to the New Jersey Department of Transportation, New York City Department of Transportation, New York Metropolitan Transportation Council, New York State Department of Transportation, and the New York State Energy and Research Development Authority and others, all while enhancing the center's theme.

Education and Workforce Development

The modern professional must combine the technical skills of engineering and planning with knowledge of economics, environmental science, management, finance, and law as well as negotiation skills, psychology and sociology. And, she/he must be computer literate, wired to the web, and knowledgeable about advances in information technology. UTRC's education and training efforts provide a multidisciplinary program of course work and experiential learning to train students and provide advanced training or retraining of practitioners to plan and manage regional transportation systems. UTRC must meet the need to educate the undergraduate and graduate student with a foundation of transportation fundamentals that allows for solving complex problems in a world much more dynamic than even a decade ago. Simultaneously, the demand for continuing education is growing – either because of professional license requirements or because the workplace demands it – and provides the opportunity to combine State of Practice education with tailored ways of delivering content.

Technology Transfer

UTRC's Technology Transfer Program goes beyond what might be considered "traditional" technology transfer activities. Its main objectives are (1) to increase the awareness and level of information concerning transportation issues facing Region 2; (2) to improve the knowledge base and approach to problem solving of the region's transportation workforce, from those operating the systems to those at the most senior level of managing the system; and by doing so, to improve the overall professional capability of the transportation workforce; (3) to stimulate discussion and debate concerning the integration of new technologies into our culture, our work and our transportation systems; (4) to provide the more traditional but extremely important job of disseminating research and project reports, studies, analysis and use of tools to the education, research and practicing community both nationally and internationally; and (5) to provide unbiased information and testimony to decision-makers concerning regional transportation issues consistent with the UTRC theme.

UTRC-RF Project No: 49111-21-21

Project Date: May 2014

Project Title: Potential Sites for Tidal Power in New Jersey

Project's Website:

<http://www.utrc2.org/research/projects/potential-tidal-power-new-jersey>

Principal Investigator:

Dr. Hansong Tang
Assistant Professor
The City College of New York, CUNY
Email: htang@ccny.cuny.edu

Co-Author(s)

- Ke Qu
- Simon Kraatz
- Wenglong Cheng

Performing Organization(s): The City College of New York

Sponsors:

New Jersey Department of Transportation (NJDOT)

University Transportation Research Center - Region 2, A Regional University Transportation Center sponsored by the U.S. Department of Transportation's Research and Innovative Technology Administration

To request a hard copy of our final reports, please send us an email at utrc@utrc2.org

Mailing Address:

University Transportation Research Center
The City College of New York
Marshak Hall, Suite 910
160 Convent Avenue
New York, NY 10031
Tel: 212-650-8051, Fax: 212-650-8374
Web: www.utrc2.org

Board of Directors

The UTRC Board of Directors consists of one or two members from each Consortium school (each school receives two votes regardless of the number of representatives on the board). The Center Director is an ex-officio member of the Board and The Center management team serves as staff to the Board.

City University of New York

Dr. Hongmian Gong - Geography
Dr. Neville A. Parker - Civil Engineering

Clarkson University

Dr. Kerop D. Janoyan - Civil Engineering

Columbia University

Dr. Raimondo Betti - Civil Engineering
Dr. Elliott Sclar - Urban and Regional Planning

Cornell University

Dr. Huaizhu (Oliver) Gao - Civil Engineering
Dr. Mark A. Turnquist - Civil Engineering

Hofstra University

Dr. Jean-Paul Rodrigue - Global Studies and Geography

Manhattan College

Dr. Anirban De - Civil & Environmental Engineering
Dominic Esposito - Research Administration

New Jersey Institute of Technology

Dr. Steven Chien - Civil Engineering
Dr. Joyoung Lee - Civil & Environmental Engineering

New York Institute of Technology

Dr. Nada Marie Anid - Engineering & Computing Sciences
Dr. Marta Panero - Engineering & Computing Sciences

New York University

Dr. Mitchell L. Moss - Urban Policy and Planning
Dr. Rae Zimmerman - Planning and Public Administration

Polytechnic Institute of NYU

Dr. John C. Falcocchio - Civil Engineering
Dr. Kaan Ozbay - Civil Engineering

Rensselaer Polytechnic Institute

Dr. José Holguín-Veras - Civil Engineering
Dr. William "Al" Wallace - Systems Engineering

Rochester Institute of Technology

Dr. J. Scott Hawker - Software Engineering
Dr. James Winebrake - Science, Technology, & Society/Public Policy

Rowan University

Dr. Yusuf Mehta - Civil Engineering
Dr. Beena Sukumaran - Civil Engineering

Rutgers University

Dr. Robert Noland - Planning and Public Policy

State University of New York

Michael M. Fancher - Nanoscience
Dr. Catherine T. Lawson - City & Regional Planning
Dr. Adel W. Sadek - Transportation Systems Engineering
Dr. Shmuel Yahalom - Economics

Stevens Institute of Technology

Dr. Sophia Hassiotis - Civil Engineering
Dr. Thomas H. Wakeman III - Civil Engineering

Syracuse University

Dr. Riyad S. Aboutaha - Civil Engineering
Dr. O. Sam Salem - Construction Engineering and Management

The College of New Jersey

Dr. Thomas M. Brennan Jr. - Civil Engineering

University of Puerto Rico - Mayagüez

Dr. Ismael Pagán-Trinidad - Civil Engineering
Dr. Didier M. Valdés-Díaz - Civil Engineering

UTRC Consortium Universities

The following universities/colleges are members of the UTRC consortium.

City University of New York (CUNY)
Clarkson University (Clarkson)
Columbia University (Columbia)
Cornell University (Cornell)
Hofstra University (Hofstra)
Manhattan College
New Jersey Institute of Technology (NJIT)
New York Institute of Technology (NYIT)
New York University (NYU)
Polytechnic Institute of NYU (Poly)
Rensselaer Polytechnic Institute (RPI)
Rochester Institute of Technology (RIT)
Rowan University (Rowan)
Rutgers University (Rutgers)*
State University of New York (SUNY)
Stevens Institute of Technology (Stevens)
Syracuse University (SU)
The College of New Jersey (TCNJ)
University of Puerto Rico - Mayagüez (UPRM)

** Member under SAFETEA-LU Legislation*

UTRC Key Staff

Dr. Camille Kamga: *Director, UTRC*
Assistant Professor of Civil Engineering, CCNY

Dr. Robert E. Paaswell: *Director Emeritus of UTRC and Distinguished Professor of Civil Engineering, The City College of New York*

Herbert Levinson: *UTRC Icon Mentor, Transportation Consultant and Professor Emeritus of Transportation*

Dr. Ellen Thorson: *Senior Research Fellow, University Transportation Research Center*

Penny Eickemeyer: *Associate Director for Research, UTRC*

Dr. Alison Conway: *Associate Director for New Initiatives and Assistant Professor of Civil Engineering*

Nadia Aslam: *Assistant Director for Technology Transfer*

Dr. Anil Yazici: *Post-doc/ Senior Researcher*

Nathalie Martinez: *Research Associate/Budget Analyst*

Final Report

Project: NJDOT 2010-15 and RFCUNY 49111-21-21

Potential Sites for Tidal Power in New Jersey

Team: Hansong Tang* (PI)
Ke Qu
Simon Kraatz
Wenglong Cheng

Department of Civil Engineering, City College
The City University of New York, New York, NY 10031
*Correspondence: 212-650-8006, htang@ccny.cuny.edu

Managers: Nazhat Aboobaker¹
Camille Kamga²
Camille Crichton-Sumners¹
Genevieve Boehm-Clifton¹

¹ Bureau of Research
New Jersey Department of Transportation,
Trenton, NJ08625, USA

² University Transportation Research Center
The City College of New York
138th Street & Convent Avenue
New York, NY 10031

May 6, 2014

Acknowledgement

The work presented in this report was sponsored by the Department of Transportation of New Jersey (NJDOT 2010-15) and the Research and Innovative Technology Administration of the U.S. Department of Transportation through the University Transportation Centers program (RFCUNY 49111-21-21). The authors thank project managers Drs. Nazhat Aboobaker, Camille Kamga, and Camille Crichton-Summers and Ms. Genevieve Boehm-Clifton for their enthusiastic support and valuable input. The authors are grateful to Dr. Changsheng Chen for his help on FVCOM. This computation of this work was carried out at CUNY HPC Center and NERSC of Dept. of Energy of the United States.

TECHNICAL REPORT STANDARD TITLE PAGE

1. Report No.	2. Government Accession No.	3. Recipient's Catalog No.	
4. Title and Subtitle Potential Tidal Power for New Jersey		5. Report Date 4/26/14	
		6. Performing Organization Code	
7. Author(s) Hansong Tang, Ke Qu, Simon Kraatz, Wenglong Cheng		8. Performing Organization Report No.	
9. Performing Organization Name and Address City College of New York, 138 th st. and Convent Ave., New York, NY 10031		10. Work Unit No.	
		11. Contract or Grant No. CUNY RF 49111-21-21	
12. Sponsoring Agency Name and Address Department of Transportation of New Jersey, University Transportation Research Center		13. Type of Report and Period Covered Final report, May, 2010 – December 2013	
		14. Sponsoring Agency Code	
15. Supplementary Notes			
16. Abstract High-resolution simulation is made to model tidal energy along the coastlines of New Jersey (NJ) and its neighbor states with an unprecedentedly fine grid. On the basis of the simulation, a thorough search is made for sites for tidal power generation, with special attention to locations near transportation infrastructures, considering factors such as power density, surface area, water depth, and environmentally sensitive zones, and it also examines effects of sea-level-rise (SLR). A list of 32 top sites with power density over 250 W/m ² are identified at the coast, and among them, 21 sites with total surface area of 13 km ² are at the NJ coast, and many sites are next to bridges. 10 favorable sites are also sorted out near ports, docks, and marinas along its coastlines. It is found that SLR could substantially affect tidal energy distribution at the identified sites, and it is a factor that has to be taken into consideration in site selections. The identified sites and estimates for their associated parameters will serve as a basis for actual development of tidal power in this region.			
17. Key Words Tidal energy, seal-level-rise, high-resolution modeling, sites for tidal power, transportation infrastructure		18. Distribution Statement	
19. Security Classif. (of this report) Unclassified	20. Security Classif. (of this page) Unclassified	21. No of Pages	22. Price

Form DOT F 1700.7 (8-69)

Disclaimer

The contents of this report reflect the views of the authors, who are responsible for the facts and the accuracy of the information presented herein. The contents do not necessarily reflect the official views or policies of the NJDOT or UTRC[, (other project sponsors),] or the Federal Highway Administration. This report does not constitute a standard, specification or regulation. This document is disseminated under the sponsorship of the Department of Transportation, University Transportation Centers Program, in the interest of information exchange. The U.S. Government [and other project sponsors] assume[s] no liability for the contents or use thereof.

Table of Contents

Acknowledgement	2
Form DOT F 1700.7 (8-69)	3
Disclaimer	4
Table of contents	5
List of figures	6
List of tables	7
1. Introduction	8
1.1 Background	8
1.2 Objectives, work scope, and deliverables	10
2 Geophysical data, environmental sensitive zones, and sea-level-rise	11
2.1 Mid-Atlantic-Bight and New Jersey shoreline	11
2.2 Bathymetry, coastlines, and rivers	12
2.3 Environmentally sensitive zone	12
2.4 Sea-level-rise and its projection	12
3 Model setup	13
3.1 Model and mesh generation	13
3.2 Boundary conditions	15
3.3 Scaling of FVCOM	15
4 Model calibration and validation	16
4.1 Model calibration	16
4.2 Mesh refinement test	18
4.3 Comparison of 2D and 3D modeling	22
5 Formulas to evaluate tidal energy	26
6 Distribution of tidal energy at NJ coast	28
6.1 Total tidal energy of coastal waters	28
6.2 Locations with strong tidal power density	30
6.3 Google Earth file implemented with tidal power density	30
7 Top site for tidal power	31
8 Top sites for tidal power near transportation facilities	41
9 Sea-level-rise effects	44
10 Concluding remarks	54
References	54
Appendix A: Observation stations	58

List of Figures

Fig. 1	Region of study	11
Fig. 2	An overall and zoom view of the 20 m mesh	13
Fig. 3	Mesh generation and refinement	14
Fig. 4	The 20 m mesh at Ocean City	14
Fig. 5	Scaling of the FVCOM on parallel computing facilities	16
Fig. 6	A comparison between computed flow and measurement	17
Fig. 7	Difference of solutions on 20 m and 50 m mesh	20
Fig. 8	Sample comparison of time histories of solutions obtained with 20 and 50 m mesh	21
Fig. 9	Difference of 3D and 2D solutions	24
Fig. 10	A model for tidal current velocity	27
Fig. 11	Instantaneous total MHK energy flux.	28
Fig. 12	Distribution of average MHK energy in the whole domain and local regions	29
Fig. 13	Power density distribution within MAB	29
Fig. 14	Top sites with regard to average power density	30
Fig. 15	The Google Earth file for distribution of tidal power	31
Fig. 16	Potential sites for tidal power	37
Fig. 17	Computation of surface area of the tidal power zone	38
Fig. 18	Locations of potential sites for tidal power generation	40
Fig. 19	Identified tidal power zones and nearby environmentally sensitive zones	40
Fig. 20	Tidal power at sites near docks, marina, and ports	43
Fig. 21	Potential sites for tidal power under SLR condition	49
Fig. 22	Potential tidal power sites that disappear and newly occur due to SLR	51
Fig. 23	Tidal power at sites near docks, marina, and ports under SLR condition	53

List of Tables

Table 1	Comparison of the computed solution and measurement	17
Table 2	Mesh convergence test	19
Table 3	Difference of solutions in time history on 20 and 50 m mesh	21
Table 4	Difference of 3D and 2D solutions in time history	24
Table 5	Potential sites for tidal power	39
Table 6	Potential sites of tidal power near bridges	41
Table 7	Potential sites of tidal power adjacent to transportation facilities	43
Table 8	Potential sites for tidal power under SLR condition	50
Table 9	Potential sites for tidal power adjacent to transportation facilities under the SLR condition.	53

1. Introduction

1.1 Background

Currently, energy demand in the world is primarily met by combustion of fossil fuels. In global energy consumption in 2007, the share of fossil fuels is 88%, which includes 35.6% oil, 23.8% natural gas, and 28.6% coal, and the remaining consists of 5.6% nuclear materials and 6.4% hydropower [1]. The heavy dependence on fossil energy now results in a difficult situation that challenges the whole world; burning of fossil fuels produces CO₂ and has led to the greenhouse effect and thus global warming and climate change [2]. A consequence of global warming and climate change is sea-level-rise (SLR), which will apparently impact coastal regions worldwide by posing dangers such as coastal flooding, imbalance of ecosystems, and infrastructure damage [3, 4, 5]. In addition, at the current rate of consumption, fossil energy is expected to be exhausted in a near future. According to an estimate for the inventory and with the exploitation rate in 2008, reserves for oil, gas, and coal can only last 40, 60, and 265 years, respectively [6].

In recent years, attention has been shifted from using fossil fuels as the primary source of energy generation to utilizing various types of clean and renewable energy to supply power [7, 8, 9]. Tidal energy is such a type of energy, and it has a significant amount imbedded in oceans. Recently, various plans and pilot projects have been implemented for tidal power generation, and there is an emerging resurgent of its development in many countries [8, 9, 10]. For instance, aiming at producing 20% of its total energy from renewable resources by 2020, which corresponds to about 35% of its electricity demand, UK is aggressively exploring renewable energy from tidal sources [11]. In US, the tidal energy development is also growing rapidly with efforts from private, public, and government sectors [12, 13]. In 2012, the Federal Energy Regulatory Commission has issued a pilot commercial license to Verdant Power's RITE project in the Eastern River in New York City, which is the first commercial license for tidal power in US [14]. In New Jersey (NJ) State, it is estimated that if only 1% of its shoreline is utilized for tidal energy production, it could contribute 500 MW or more power based on presently available technology during the next two to three years, while adding over one billion US dollars to its economy in the next decade [15].

The first as well as a crucial step in actual tidal power development will be a reliable survey of spatial distribution and temporal variation of tidal energy along coastlines and, on this basis, selection of the best sites for tidal power generation. For this purpose, in recent years, many countries around the world are making surveys on tidal energy along their coastlines, and databases for potential regions for power generation have been created. For example, an investigation has been made on tidal current energy along the entire coast of Ireland, and its total tidal power was assessed at 230 TWh/y [16]. It was computed that UK had 95WTh/y in theoretical tidal stream energy, and recently another project of a complete survey has been initiated in the country [17, 18]. An analysis was made to review tidal energy at more than 100 sites of Norway, and it

estimated that they yielded a theoretical resource on the order of 17 TWh [19]. On the basis of studies at a big portion of its coastal zones, it was projected that the average power available from tidal currents in China exceeded 122 TWh/y [10]. An inventory was presented on tidal energy in each of states in US, and it was stated that totally the nation had 250 TWh/y in tidal current energy [20, 21]. Additionally, a number of investigations have been made to assess tidal energy at local sites. Among many such local sites, examples are the Alas Strait of Indonesia [22], the Kinmen Island of Taiwan [23], the Cook Strait of New Zealand [24], the Ri'a de Muros on the north-western coast of Spain [25], the Severn Estuary in UK [26], the Minas Passage in the Bay of Fundy in Canada [27], and the Beaufort River of South Carolina, US [28].

Nevertheless, above and other existing surveys are preliminary and cannot meet the needs of actual projects, and more advanced techniques and approaches are necessary and detailed investigations with desired resolution and accuracy are yet to be made to serve the development of tidal power generation and also the evaluation of its impact on environments. For instance, as indicated in [19], although it is recognized that there is a considerable tidal energy resource in Norwegian waters, how much of this resource could be utilized is still unknown, and clearly a further study of the resource is necessary. Generally, in the theoretically estimated tidal energy potential, only a fraction can be realized in practice because of physical constraints on water depth, installation of turbines, potential environmental impact, etc., and influence of these constraints have to be further evaluated using more detailed and advanced methods [19, 27]. It is asserted that the current situation is the resolution of surveys, especially in nearshore regions and tributaries, is such that the resource may be underestimated and should therefore be supplemented by detailed models or site-specific measurements [17]. In the aforementioned nationwide survey of tidal energy in US, it is admitted that its approach cannot detect tidal energy at a number of local sites in different states, and a further assessment has to be made with better modeling or measurement [20]. In consistency with this status, NJ State has to initiate a research project to assess tidal energy at its local coast, which is a pilot effort of its type in view that it targets a thorough search for nearshore tidal energy and top ranked sites, with emphasis on locations near transportation systems in marinas, docks, jetties, bridges, and infrastructure where known tidal technology could be sited [15]. Because of needs in actual tidal power generation projects, also in view of the current status of evolution in tidal energy survey, now it is necessary and the time as well to improve our assessment of tidal energy and bring it to a new level with more details and a better accuracy. For a detailed review on history and current status, as well as difficulties and methods, i.e., analytical approach, numerical method, and field measurement, for tidal energy survey, the reader is referred to [29].

1.2 Objectives, work scope, and deliverables

Towards tidal power generation, NJDOT called a comprehensive assessment for tidal energy development in NJ State. In the RFP of Project 2010-15, the following tasks were targeted [15]:

1. Identification and evaluation of tidal zones along the coast of New Jersey.
2. Identify known tidal technology that could be utilized in New Jersey.
3. Identification of potential locations in marinas, docks, jetties, bridges and other shorelines infrastructure where known tidal technology could be sited. Also identify any exclusionary conditions or zones.
4. Estimates of water speeds available at potential sites from river and tidal flows along with water depth data that would result in an accurate assessment of total potential power output.
5. Calculation of tidal power potential from each tidal zone along the New Jersey coast.
6. Roadmap potential pathways and strategic partners, including New Jersey public utilities, for tidal power development in New Jersey based on all of the above.
7. Recommend 20 primary locations based on the potential for project success as well as the value to the State and the New Jersey's Marine Transportation System.

Tidal power development at marine transportation systems and facilities as well as bridges is of particularly interest.

In correspondence with above targeted tasks, this project aims at a thorough survey of tidal energy, especially marine hydrokinetic (MHK) energy, along NJ coast. In particular, according to the above listed tasks, it searches for potential tidal power sites, with emphasis on locations near transportation facilities, considering not only available tidal power but also constraints including desired water depth and environmentally sensitive zones. In addition, since tidal power generation is a long time business, this project also examines the potential influence on tidal power introduced by SLR as a consequence of climate change.

Originally, the scope of work for this project consisted of computer modeling and field measurement. At its late stage, the measurement activity was canceled due to budget cut/termination. Nevertheless, all of above tasks have been basically finished except contents in items 2 and 6 listed above, and the results of this project are reported in the following sections. Another analysis of top sites for tidal power is reported by the sub-contractor of this project [30].

The deliverables of this project are as follows:

1. Final project report (this report)
2. A Google Earth file with tidal energy and other information
3. Website http://www-ce.cuny.cuny.edu/cfd/NJDOT_UTRC_project.html (in construction)
4. Journal publications: a) Tang HS, Kraatz S, Qu K, Chen GQ, Aboobaker N, and Jiang CB. High-resolution survey for tidal energy and influence of sea-level-rise: a case study at coast

of New Jersey, USA. Renewable & Sustainable Energy Reviews 2014; 32:960–982. b) Tang HS, Qu K, Chen GQ, Kraatz S, Aboobaker N, and Jiang CB. Potential sites for tidal power generation: A thorough search at coast of New Jersey, USA. Renewable & Sustainable Energy Reviews 2014, Submitted.

5. A report from the sub-contractor of this project [30].

The readers may contact the PI for information on the deliverables.

2. Geophysical data, Environmentally Sensitive Zones, and Sea-Level-Rise

2.1 Mid-Atlantic-Bight and New Jersey shoreline

The region of study covers the Mid-Atlantic-Bight (MAB); it starts from Massachusetts and ends at Virginia, ranging from latitude of 36.8 N to 41.3 N and longitude of 77.3 W to 71.3W (Fig. 1). In the nearshore region, the water depth in most part of the domain is less than 30 m. The seafloor extends outwards with a mild slope over 100 km from the inlet of the Chesapeake Bay and over 170 km from the Connecticut shoreline. The seabed slope becomes fairly steep near the edge of the continental shelf; where over a distance of 20 km the water depth increases up to 2000 m. The coastline of NJ runs from the mouth of Hudson River to the eastern side of the Delaware Bay, with a water system consisting of many beaches, bays, and rivers in between, and they are measured 130 miles in general coastline and 1,792 miles in tidal shoreline [31].

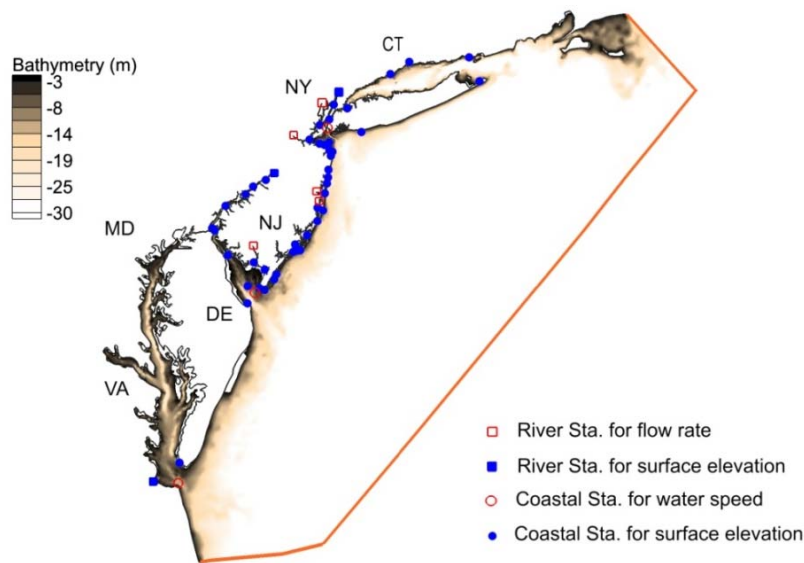


Fig. 1 Region of study. Symbols are observation stations, and the red line is an open boundary where astronomic tide conditions will be imposed.

2.2 Bathymetry, coastlines, and rivers

Bathymetry data from NOAA NGDC is available for most part of the MAB region, except for small channels and rivers, and it will be used in this study [32, 33]. The NOAA bathymetry data has a resolution of about 100 meters for majority of nearshore zones, and it presents a coarser resolution for regions further away from the coast. NOAA's VDATUM is used to convert the bathymetry data to the common vertical datum NAVD88 [34].

The seashore boundaries are defined by the NOAA high-resolution composite vector shoreline [35]. In addition, at the locations where small rivers are not included in the high-resolution data set, NOAA medium resolution coastlines are used [36]. Along the coastlines of the region, there are a number of rivers with water flowing into the ocean [37]. However, as marked in Fig. 1, flows of only eight of them will be included in the study of this paper, since others are either located far away from the region of interest or do not carry a significant amount of discharge.

2.3 Environmentally sensitive zone

NJ Department of Environmental Protection has identified the Environmentally Sensitive Planning Area. Such area contains large contiguous land with irreplaceable resources including valuable ecosystems, geological features, and wildlife habitats along NJ coast, and thus it is protected and tidal power development cannot be implemented in it. A map of the area, in particular, the Coastal Environmentally Sensitive Planning Area, is available at the website of GIS of NJDEP [38], and it will be utilized in this study.

2.4 Sea-level-rise and its projection

It is well recognized that the global mean sea level is now increasing with time, and that the MAB region will experience a SLR that is greater than the global average value. Research shows that, mainly due to effects of climate change such as ice sheet melting, global SLR is at an alarming rate of 0.18 cm/year during 1961-2003 and even a higher value of 0.3 cm/year during 1993-2003 [39]. According to a recent study by Yin et al. [40], climate change is expected to cause the sea level along the northeastern U.S. coastlines, including those of the MAB, to rise almost twice as fast as global sea level during this century. It is projected that the median range of the global SLR over next 100 years will range from 0.2 to 0.6 m, and it could range from 0.8 to 2 m by 2100 under unfavorable conditions [41,42]. In this project, SLR scenarios of 0.5 m and 1 m are considered, which roughly correspond to the estimated median values for SLR in the region of study in 50 and 100 years, respectively [3,29].

3. Model Setup

3.1 Model and mesh generation

In view of highly irregular shapes of shorelines of coastal waters and streams and the need for high-resolution meshes at nearshore regions, the version 2.7 finite volume coastal ocean model (FVCOM) is used to simulate the tidal flows in this paper. FVCOM solves the geophysical fluid dynamics equations in conjunction with the Mellor and Yamada level-2.5 turbulence closure, and it has a two dimensional (2D) external mode and a three dimensional (3D) internal mode [43]. Since the model uses a triangle mesh in the horizontal plane, it can easily deal with complicated shorelines of coastal waters and borders of tributaries with high-resolution meshes. In addition, the governing equations are discretized using a finite volume method, and this results in conservative schemes that preserve mass and momentum conservation with good accuracy, which are appealing features in numerical simulation of complicated nearshore flows.

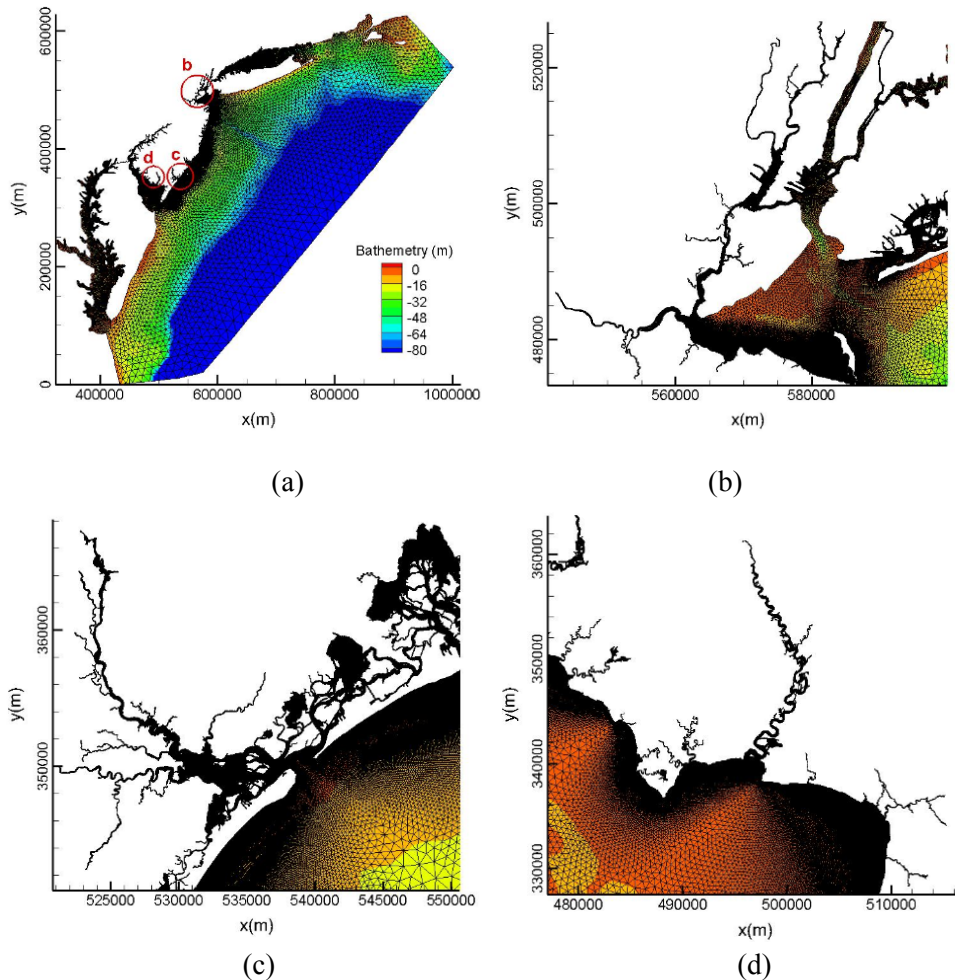


Fig. 2 An overall and zoom view of the 20 m mesh. (a) Global mesh. (b) Mesh at b in (a). (c) Mesh at c in (a). (d) Mesh at d in (a).

A triangle mesh is generated with 50 m resolution along all flow boundaries within NJ, and local refinement with grid spacing as small as less than 10 m is made to resolve flows within small

tributaries (Fig.2a). For the purpose to reduce the total number of elements, larger grid spacing is used in most part of regions other than NJ but no significant alteration is made for the shapes of the borders of waters. A few locations far away from the NJ coastlines are meshed with fine grid spacing, and examples are the south shore of the Long Island Sound and the shoreline of Jamaica Bay, where grid spacing of 50 m or less is used. Hereafter, this mesh is donated as the 50 m mesh, and it has 2.06 million nodes and 3.8 million elements in the horizontal plane. On the basis of the 50 m mesh, in order to resolve small-scale flows at potential sites for tidal power generation, a finer mesh is also made by reducing the distance between nodes along all of the borders of the NJ coastal waters in the 50 m mesh from 50 m to 20 m (Fig. 2b). An overall and zoom view of this mesh are shown in Fig. 3. Hereafter, this fine mesh is referred as to the 20 m mesh, and it has 3.3 million nodes and 6.3 million elements. This mesh has fine resolution for channels, ponds, tributaries, etc., and it is expected to be able to resolve local flows at scales of power generation equipments (Fig. 4).

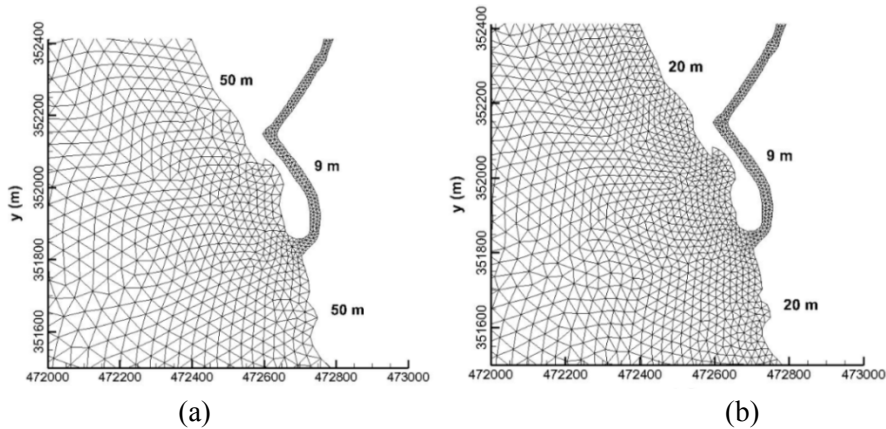


Fig. 3 Mesh generation and refinement. In the figure, $(x,y)=(x^*,y^*-4 \times 10^6)$, where (x^*,y^*) is the coordinate in UTM, NAD83, Meters, ZONE = 18.0. The numbers in the figure indicate grid spacing. (a) The 50 m mesh. (b) The 20 m mesh.

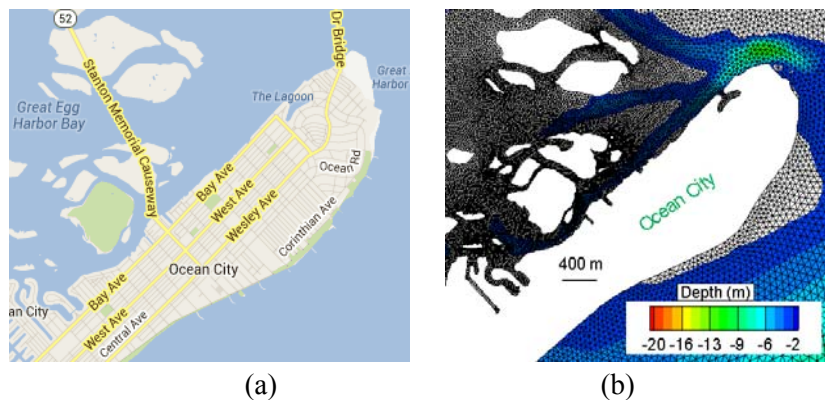


Fig. 4 The 20 m mesh at Ocean City. (a) Map of the city. (b) Mesh at the city.

3.2 Boundary conditions

At the open boundary, the red line as shown in Fig. 1, water surface elevation is specified with the astronomic tide conditions provided by software OTPS. The software uses the TPXO7.2 global ocean tidal model. The model is calibrated with measurements obtained from the TOPEX/Poseidon and Jason satellites, and it includes 13 tidal components of the water surface elevation: eight primary (M2, S2, N2, K2, K1, O1, P1, Q1), two long period (Mf, Mm), and three non-linear (M4, MS4, MN4) constituents [44]. At the locations marked as the open red squares in Fig. 1, flow discharges from Raritan River, Passaic River, Tom's River, Cedar Creek, and Maurice River are determined by recorded field data. In addition, at the James River near the mouth of Chesapeake Bay, Hudson River near Washington Bridge, and Delaware River at Trenton, which are marked as filled blue squares in Fig. 1, water surface elevation is imposed according to observation data [45]. In order to maintain numerical stability, a weak sponge layer with 10^{-3} for the sponge coefficient and 5km for the sponge radius has been used at the open boundary [46].

Generally speaking, wind affects coastal flows. In view that wind is usually random in both direction and magnitude, and also the fact that tidal power generation utilizes energy due to regular astronomic tides, this study ignores the effects of wind, which, as indicated in [28], is in consistent with earlier investigations. Actually, observation data indicate that average wind in the MAB is rather weak [47]. In addition, effect of density stratification is ignored, and this is reasonable for flows in nearshore regions, where tidal energy extraction is usually implemented.

3.3 Scaling of FVCOM

Since this research requires many model runs with very large numbers of mesh elements, it involves intensive computing, and computational power and efficiency become a crucial issue. In order to achieve desired computational power, the model runs are carried out on parallel computing facility SALK at City University of New York (CUNY) HPC Center and HOPPER at National Energy Research Scientific Computing Center (NERSC) of Dept. of Energy, both of which are Cray computers [48,49]. The scaling of FVCOM on SALK is shown in Fig. 5a. It is seen in the figure that both of the 2D and 3D mode of FVCOM can scale ideally, as a straight line, up to 1024 cores. This scaling is achieved in simulation of the flow within the MAB using the 20 m mesh and time step 0.1 s. Fig. 5b presents the scaling of the FVCOM 2D mode on HOPPER. The figure indicates that the model scales ideally up to 1920 cores and reaches its best performance at 3,840 cores. If 1024 cores are used, it takes about 2.6 days to finish a 2D mode run using the 20 m mesh and time step 0.1 s on SALK, and the computation will last for 3 days on HOPPER. In this project, model runs are made using the numbers of cores that are not only available but also permit best efficiency estimated by the scaling of FVCOM.

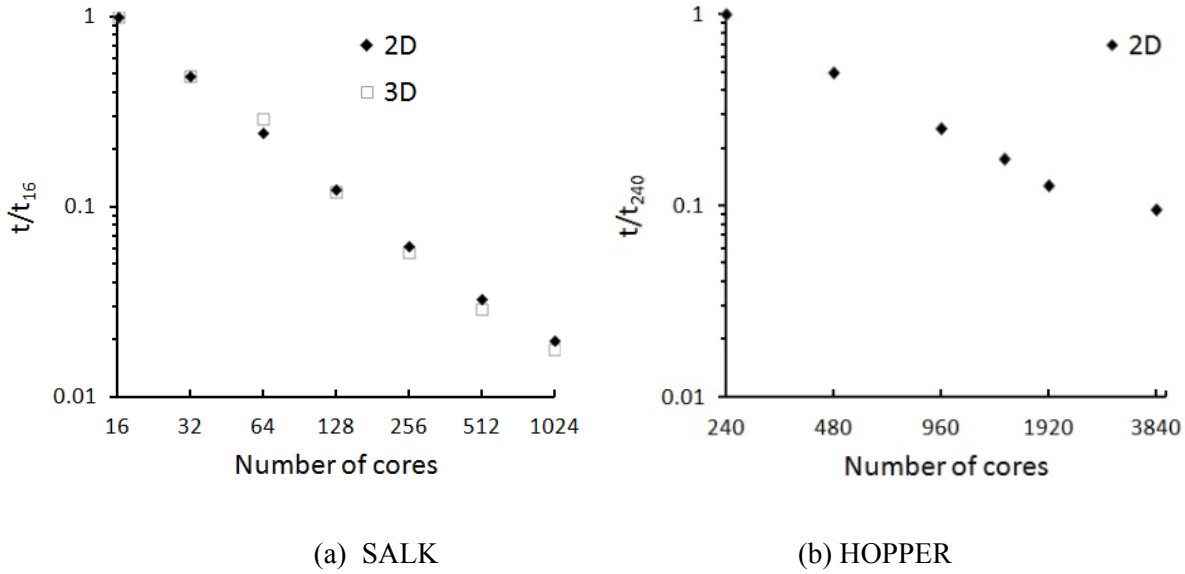


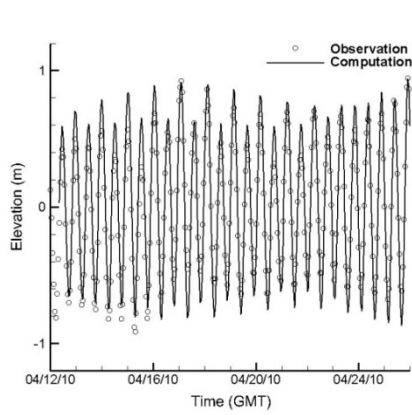
Fig. 5 Scaling of the FVCOM on parallel computing facilities. t_{16} and t_{240} represent the time needed on 16 and 240 cores, respectively.

4. Model Calibration and Validation

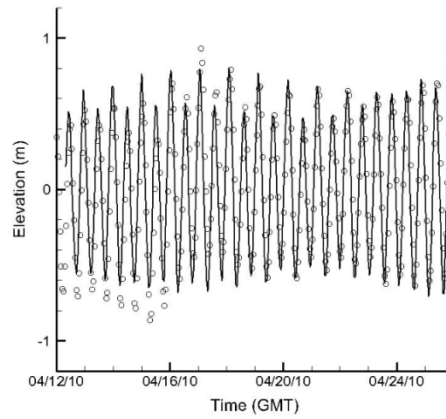
4.1 Model calibration

Observation data for the coastal flows has been collected from various sources, and measurements at totally 47 coastal stations will be used for this research [36,45,50]. Among the 47 stations, three measure currents, and the remaining stations record surface elevations. These stations scatter at the coastal regions ranging from Long Island Sound to Chesapeake Bay, and most of them are in the NJ waters within 1km from its shoreline. The locations of the stations are shown in Fig. 1 and given in Appendix, and more details for the stations, plus those for above bathymetry, coastlines, used in the model setup can be found in [51].

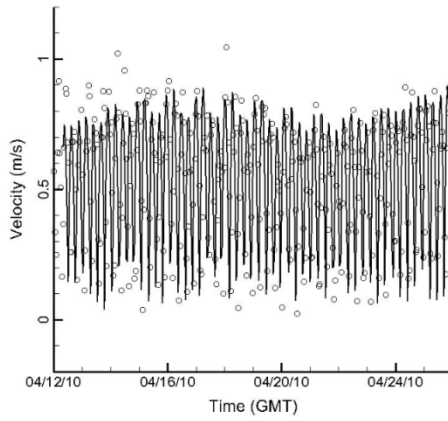
In order to calibrate the setup of the model, its solution for the flow during 8:00 am on April 12, and 12:00 pm on April 25, 2010 on the 20 m mesh and with time step 0.1 s is compared against observation data at the 47 observation stations along the coastlines (Appendix A). Station 10, 12, and 27 measure current velocity, and the rest record water surface elevation. For the purpose to exclude the effects of transient stages in the computation, the model run starts from 0:00 am on April 10, 2010. Overall the computed solution, especially its water surface elevation, is in a good agreement with the observation data. A sample comparison between the simulation and the observation data is shown in Fig. 6, and a quantitative difference between them is presented in Table 1.



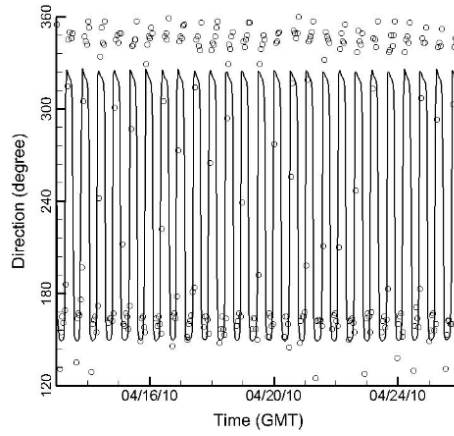
(a) Atlantic City



(b) Point Pleasant.



(c) Brown Shoal Light



(d) Brown Shoal Light

Fig. 6 A comparison between the computed flow and measurement.

Table 1 Comparison of the computed solution and measurement at the 47 observation stations. In the table, f can be water surface elevation, or velocity magnitude, or its direction, and subscript c and o refer to computed solution and observation, respectively, and N is the total number of the stations. The unit of f is m, or m/s, or degree, depending on the meaning that it stands for.

Station	$\ f_c - f_o\ _2 / \sqrt{N}$
1	0.293
2	0.174
3	0.090
4	0.086

Station	$\ f_c - f_o\ _2 / \sqrt{N}$	
25	0.188	
26	0.167	
27	Vel	0.353
	Dir	39.779
28	0.294	

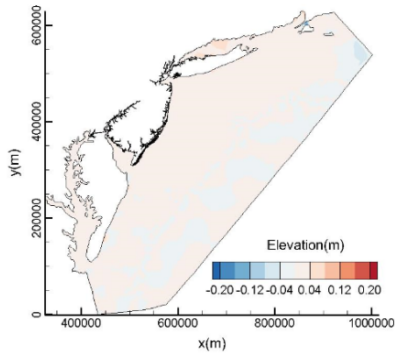
5	0.165	
6	0.181	
7	0.112	
8	0.301	
9	0.098	
10	Vel	0.289
	Dir	59.126
11	0.112	
12	Vel	0.226
	Dir	68.960
13	0.122	
14	0.206	
15	0.104	
16	0.131	
17	0.137	
18	0.123	
19	0.125	
20	0.149	
21	0.376	
22	0.201	
23	0.134	
24	0.180	
29	0.144	
30	0.130	
31	0.238	
32	0.214	
33	0.246	
34	0.128	
35	0.099	
36	0.372	
37	0.119	
38	0.138	
39	0.115	
40	0.132	
41	0.182	
42	0.193	
43	0.214	
44	0.202	
45	0.130	
46	0.083	
47	0.148	

4.2 Mesh refinement test

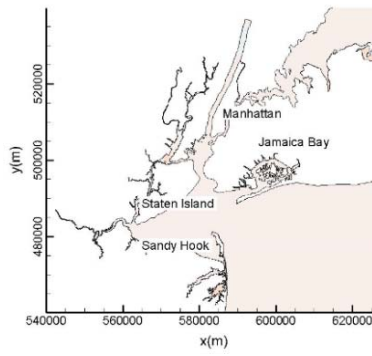
Computations have been made on different meshes to ensure mesh independent solutions, and a mesh convergence test using the 2D FVCOM mode for the flow during 8:00 am on April 12 and 12:00 pm on April 25, 2010 on the 50 m and 20 m mesh with time step 0.2 s and 0.1 s, respectively, is shown in Table 2, which shows that the solutions on the two meshes are indeed close. In calculation of the difference, the solution on the 20 m mesh is interpolated onto the 50 m mesh, and then the resulting interpolated values on the 50 mesh is subtracted from the solution computed on the 50 m mesh. It should be noted that techniques are available to further validate the mesh convergence of numerical solutions by comparison of solutions obtained with different grid spacing and time steps (e.g., [52]). A visualization of the difference of the solutions at 12:00 pm on April 25, 2010 on the 50 m and 20 m mesh, the latter minus the former, is presented in Fig. 7. It is seen from the table and the figure that the two solutions generally differ little in spatial distributions, the difference in general being bounded by -0.1 m and 0.1 m in water surface elevation and -0.1 m/s and 0.1 m/s in water speed, respectively.

Table 2 Mesh convergence test. η , u , and v are water surface elevation, velocity in x , and velocity in y direction, respectively, at 12:00 pm on April 25, 2010 and subscript 50 and 20 indicate solutions on the 50 and 20 m mesh, respectively. A is the total area of the flow.

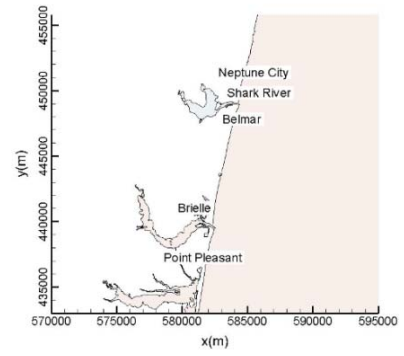
$\ \eta_{50} - \eta_{20}\ _2 / \sqrt{A}$ (m)	$\ u_{50} - v_{20}\ _2 / \sqrt{A}$ (m/s)	$\ v_{50} - v_{20}\ _2 / \sqrt{A}$ (m/s)
1.43E-02	2.75E-02	3.90E-02



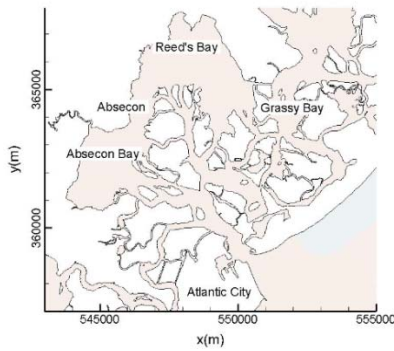
(a)



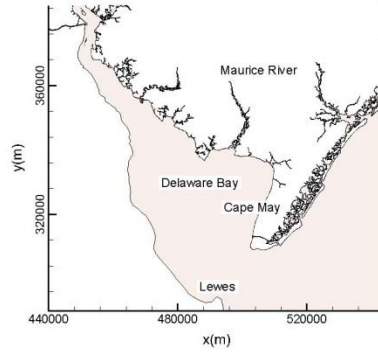
(b)



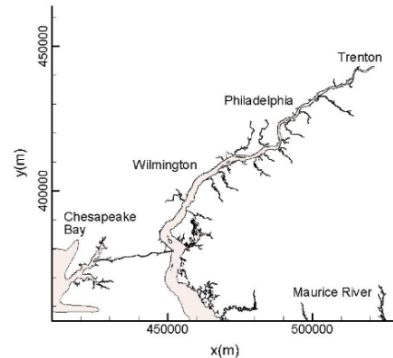
(c)



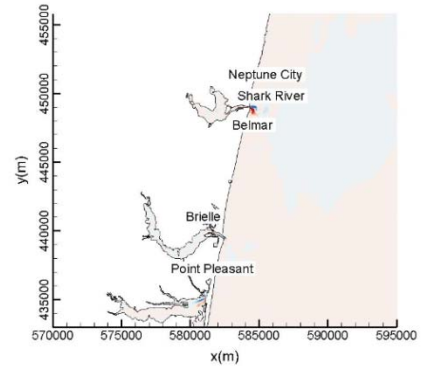
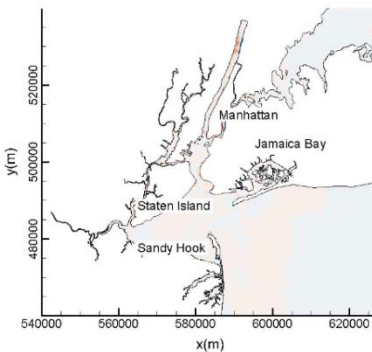
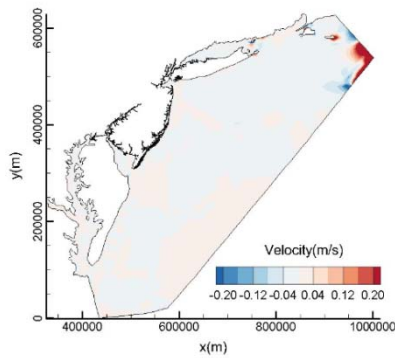
(d)



(e)



(f)



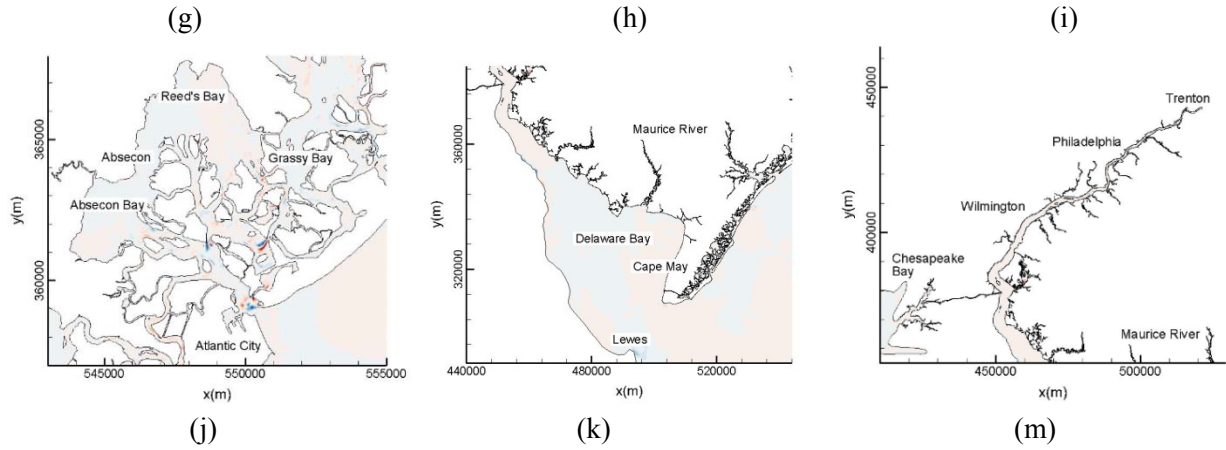
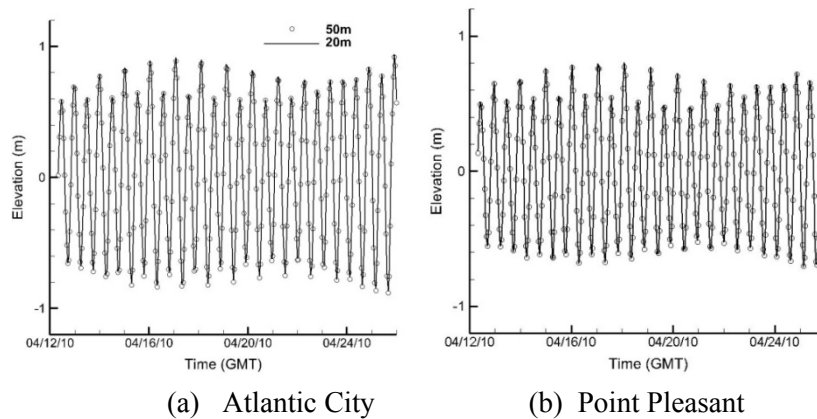
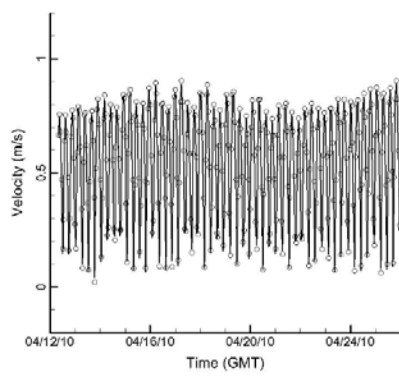


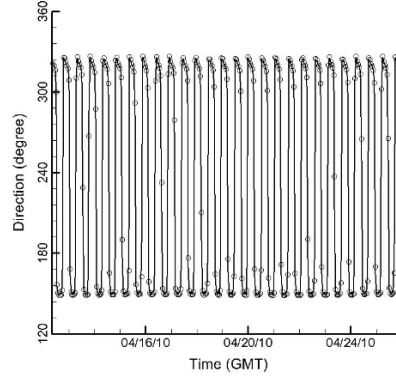
Fig. 7 Difference of solutions on 20 m and 50 m mesh, at 12:00 pm on April 25, 2010. (a) – (f) Difference in water surface elevation. (g)-(m) Difference in velocity magnitude.

Comparison of the solutions obtained on the 20 and 50 m mesh is also made with regard to their temporal evolutions. A direct comparison between the time histories of the two solutions at two observation stations is shown in Fig. 8. The figure shows that time histories of the two solutions at these two sites are indeed very close, although the ratio of grid spacing of their mesh is 2.5 times in nearshore regions. For a more comprehensive comparison, Table 3 presents a quantitative comparison of the time histories at all of the 47 observation stations. The table shows that the temporal evolutions of the two solutions are about the same; the two solutions are very close in water surface elevation, while their difference in velocity seems bigger at a few stations. All of above confirms that the 2D solution on 20 m mesh can be considered as a mesh independent solution.





(c) Brown Shoal Light



(d) Brown Shoal Light

Fig. 8 Sample comparison of time histories of solutions obtained with 20 and 50 m mesh.

Table 3 Difference of solutions in time history on 20 and 50 m mesh at the 47 observation stations.

Station	$\ \eta_{50} - \eta_{20} \ _2 / \sqrt{N}$ (m)	$\ u_{50} - u_{20} \ _2 / \sqrt{N}$ (m/s)	$\ v_{50} - v_{20} \ _2 / \sqrt{N}$ (m/s)
1	0.011	0.001	0.002
2	0.019	0.016	0.009
3	0.011	0.005	0.007
4	0.011	0.004	0.008
5	0.015	0.010	0.021
6	0.023	0.077	0.037
7	0.016	0.027	0.023
8	0.022	0.006	0.005
9	0.036	0.008	0.009
10	0.015	0.015	0.009
11	0.014	0.221	0.202
12	0.012	0.026	0.005
13	0.014	0.122	0.017
14	0.020	0.035	0.016
15	0.010	0.008	0.011
16	0.012	0.023	0.043
17	0.036	0.054	0.039
18	0.026	0.040	0.217
19	0.013	0.010	0.021
20	0.015	0.085	0.011
21	0.029	0.026	0.043
22	0.022	0.000	0.001

23	0.015	0.014	0.014
24	0.036	0.126	0.095
25	0.017	0.023	0.03
26	0.007	0.008	0.005
27	0.012	0.051	0.037
28	0.023	0.032	0.035
29	0.021	0.031	0.011
30	0.017	0.006	0.006
31	0.013	0.006	0.002
32	0.017	0.012	0.027
33	0.014	0.007	0.006
34	0.015	0.019	0.02
35	0.042	0.041	0.308
36	0.018	0.002	0.005
37	0.015	0.010	0.013
38	0.057	0.032	0.042
39	0.011	0.003	0.009
40	0.016	0.005	0.005
41	0.014	0.015	0.011
42	0.014	0.015	0.011
43	0.014	0.023	0.016
44	0.014	0.029	0.056
45	0.011	0.014	0.008
46	0.010	0.114	0.016
47	0.017	0.002	0.009

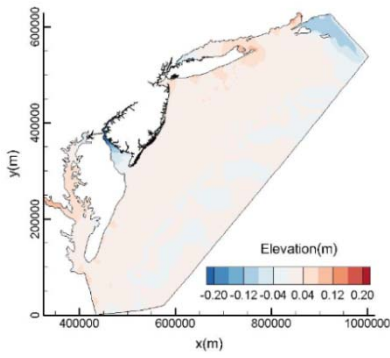
4.3 Comparison of 2D and 3D modeling

In order to evaluate its 3D effects, a computation for the flow during April 12 and April 25, 2010 is made using the 3D mode of FVCOM, the 50 m mesh with 6 σ -layers, time step 0.05s and 0.5s for the external and internal mode, respectively, and other related parameters adopted in the 2D modeling. An instantaneous difference of the 3D solution, in particular its 2D mode solution, with that obtained by the 2D mode and 50 m mesh, the former minus the latter, is shown in Fig. 9. It is seen that the two solutions indeed have difference in their spatial distributions, and this indicates the 3D effects play a role at zones where the difference is big. However, the figure shows that in general the difference is within ± 0.2 m/s in velocity and ± 0.2 m in elevation. Table 4 further quantifies the difference of the two solutions in time at the 47 observation stations, in which

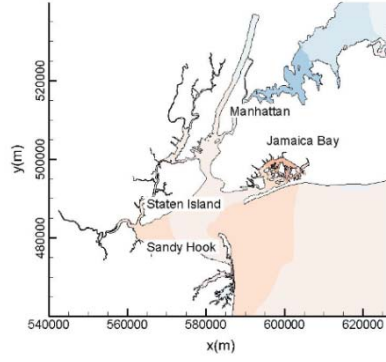
$$DM = \sqrt{\frac{1}{N} \sum_{i=1}^N [f_i^{3D} - f_i^{2D}]^2}, \quad (1)$$

$$DP = \frac{1}{N} \sum_{i=1}^N |t_i^{3D} - t_i^{2D}|, \quad (2)$$

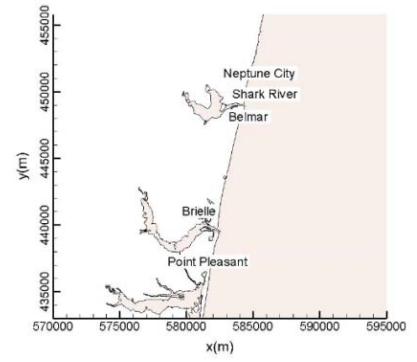
where i and N are respectively the i th occurrence of maximum or minimum of water surface elevation or speed and the total number of such occurrences during the simulation duration, f and t are respectively the magnitude of the maximum or the minimum and the time it happens, and superscript 3D and 2D denote solution on 3D and 2D mesh, respectively. Basically, MD and DP represent the difference of two solutions in magnitude and phase, and they are used by other authors [53]. As shown in Table 4, the 3D and 2D solution are close in their evolution in time in view of their magnitudes and phases. It is interestingly noticed that, at most of the 47 stations, DP is positive for water elevation and negative for flow speed, or, the 3D solution is faster than the 2D solution in phase of surface elevation, but slower in phase of flow speed.



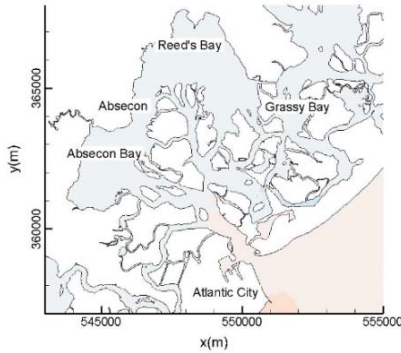
(a)



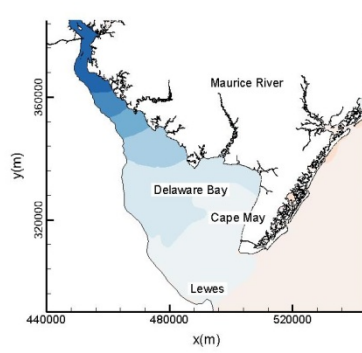
(b)



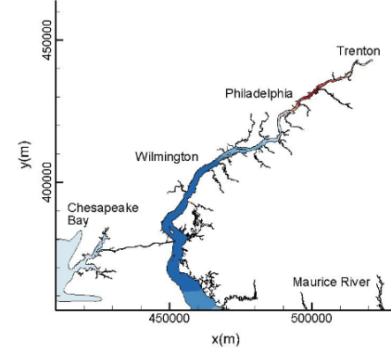
(c)



(d)



(e)



(f)

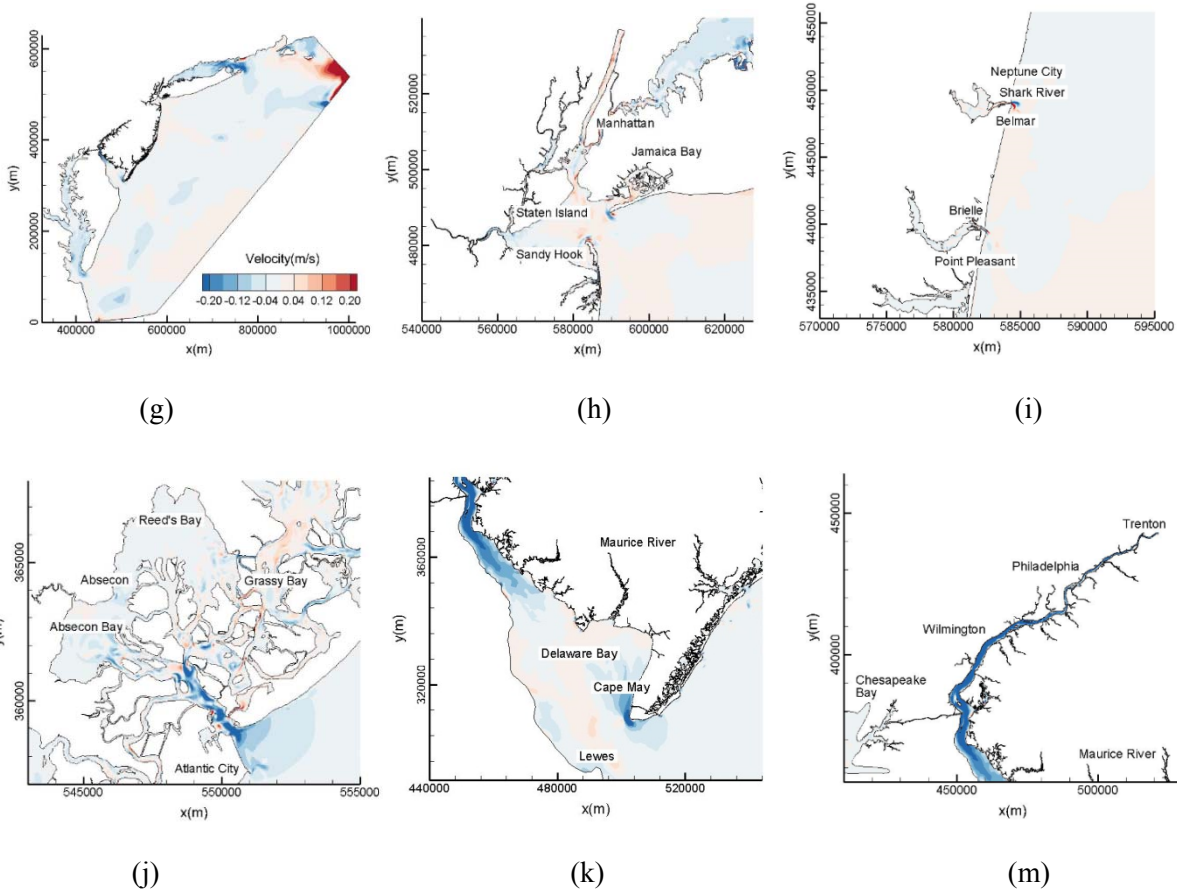


Fig 9 Difference of 3D and 2D solutions, at 12:00 pm on April 25, 2010 on the 50 m mesh. (a) – (f) Difference in water surface elevation. (g)-(m) Difference in velocity magnitude.

Table 4 Difference of 3D and 2D solutions in time history at the 47 observation stations obtained with the 50 m mesh.

Station	Elevation		Velocity	
	DM (m)	DP (min)	DM (m)	DP (min)
1	0.028	14.118	0.003	4.687
2	0.015	0.000	0.008	16.593
3	0.014	-1.081	0.006	18.933
4	0.011	2.380	0.016	-9.374
5	0.023	5.950	0.014	-30.721
6	0.032	6.816	0.067	-11.893
7	0.061	-10.601	0.024	-23.864
8	0.158	-9.086	0.036	-10.673
9	0.075	9.374	0.014	12.583
10	0.064	4.651	0.133	-7.659

11	0.036	6.706	0.342	5.625
12	0.017	3.570	0.040	-22.347
13	0.068	7.897	0.030	18.438
14	0.021	5.733	0.022	21.838
15	0.018	4.633	0.139	-7.171
16	0.034	6.924	0.079	30.594
17	0.068	4.543	0.035	-4.000
18	0.017	6.924	0.098	-16.419
19	0.034	4.543	0.014	-17.636
20	0.030	5.733	0.055	-1.223
21	0.185	-2.272	0.060	28.928
22	0.046	3.246	0.000	-18.173
23	0.048	2.272	0.057	29.388
24	0.024	-0.108	0.160	2.961
25	0.043	8.162	0.116	-6.538
26	0.010	-47.596	0.034	6.343
27	0.042	4.759	0.049	-25.171
28	0.146	-11.359	0.087	56.706
29	0.109	348.199	0.071	-12.443
30	0.045	3.354	0.063	19.492
31	0.024	-3.570	0.012	-3.963
32	0.022	-1.081	0.014	-23.980
33	0.029	3.529	0.008	7.462
34	0.020	9.302	0.009	-0.331
35	0.046	3.462	0.298	-21.491
36	0.111	13.738	0.006	3.028
37	0.022	5.950	0.014	-34.358
38	0.012	-1.081	0.042	-8.372
39	0.007	2.055	0.008	26.636
40	0.133	14.007	0.142	20.000
41	0.192	15.037	0.144	-9.317
42	0.202	9.302	0.154	-5.893
43	0.258	16.118	0.067	-7.671
44	0.220	19.796	0.101	-36.030
45	0.162	23.603	0.169	-1.820
46	0.113	10.809	0.174	-2.251
47	0.074	4.435	0.079	10.800

As illustrated in the above paragraph, the 3D and 2D solution are close in both spatial and temporal distribution. In view that a 3D modeling is very expensive and nearshore flows are usually well-mixed in the vertical direction, this paper ignores 3D effects and, hereafter, it focuses on 2D

modeling on the 20 m mesh and only presents solutions for vertical average flows, which is widely used in previous investigations (e.g., [53]).

5. Formulas to Evaluate Tidal Energy

The kinetic energy E , or MHK energy, within a flow domain Ω is evaluated as

$$E = \int_{\Omega} \frac{1}{2} \rho V^2 d\Omega, \quad (3)$$

where ρ is the water density and V is the depth average velocity magnitude. The averaged MHK energy \bar{E} within the domain over time T reads as

$$\bar{E} = \frac{1}{T} \int_0^T \int_{\Omega} \frac{1}{2} \rho V^2 d\Omega dt. \quad (4)$$

In evaluation of MHK energy, tidal power density P , also called tidal power, is usually considered:

$$P = \frac{1}{2} \rho V^3, \quad (5)$$

which is actually the MHK energy passing unit cross-section area during unit time. The averaged power density \bar{P} over a period T at a location is computed as

$$\bar{P} = \frac{1}{T} \int_0^T \frac{1}{2} \rho V^3 dt. \quad (6)$$

In addition, along a line Γ within certain distance from a coastline, the total MHK energy flux, or, the total MHK energy across it, will be

$$\hat{P} = \int_{\Gamma} \frac{1}{2} \rho V^3 d\Gamma, \quad (7)$$

which is frequently used to evaluate total tidal power at the coastal region, and the average of the total flux is

$$\tilde{P} = \frac{1}{T} \int_0^T \int_{\Gamma} \frac{1}{2} \rho V^3 d\Gamma dt. \quad (8)$$

It should be noted that V is a function of time, and not every piece of its value will contribute in actual power generation; according to their power curve, tidal power generation equipments have a cut in velocity, below which they do not generate power, and a cut out velocity, above which the turbines are shut down [54,55]. In addition, in general V will be altered after power generation facilities are installed in water. In this study, these factors will not be considered.

Generally speaking, a tidal current alternates its direction and velocity magnitude. Assuming two tides during a day and a simple model for V as shown in Fig. 10, formula (6) yields

$$\frac{1}{3} \int_0^3 \left(\frac{1}{2} \rho \left(\frac{V_p t}{3} \right)^3 \right) dt = \bar{P}, \quad (9)$$

from which an expression for the peak value of V_p is derived as

$$V_p = \sqrt[3]{\frac{8\bar{P}}{\rho}}. \quad (10)$$

Apparently, in the simplified model, the mean velocity V_m is

$$V_m = 0.5V_p. \quad (11)$$

Expression (5) and (6) will be used to estimate peak value and mean value, respectively, of a tidal current from a given value of \bar{P} .

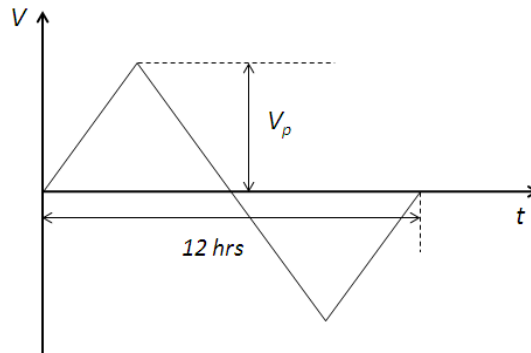


Fig. 10 A model for tidal current velocity.

6. Distribution of Tidal Energy at NJ Coast

6.1 Total tidal energy of coastal waters

The total MHK energy, E , within the computational domain, which is roughly the whole MAB region, is computed using the 2D solution on the 20 m mesh during April 12 and 25, 2010. The computed E fluctuates with time because of tides, and $4.6 \times 10^{13} < E < 1.9 \times 10^{14}$ J, with 14-day average $\bar{E} = 1.1 \times 10^{14}$ J. Considering the water body of 2 km within the NJ coastlines, the corresponding values are computed as $4.1 \times 10^{11} < E < 2.0 \times 10^{12}$ J, with average $\bar{E} = 1.1 \times 10^{12}$ J. In addition, the total MHK energy flux \hat{P} across the open boundary of the computation domain, the red line in Fig. 1, as well as that along the line 2 km from the coast of NJ are also computed (Fig. 11). The average values of \hat{P} , or \tilde{P} , are respectively 2.1×10^9 W and 1.4×10^8 W along the open boundary and the 2 km line, and the two numbers reflect estimates of tidal energy within MAB and NJ coast.

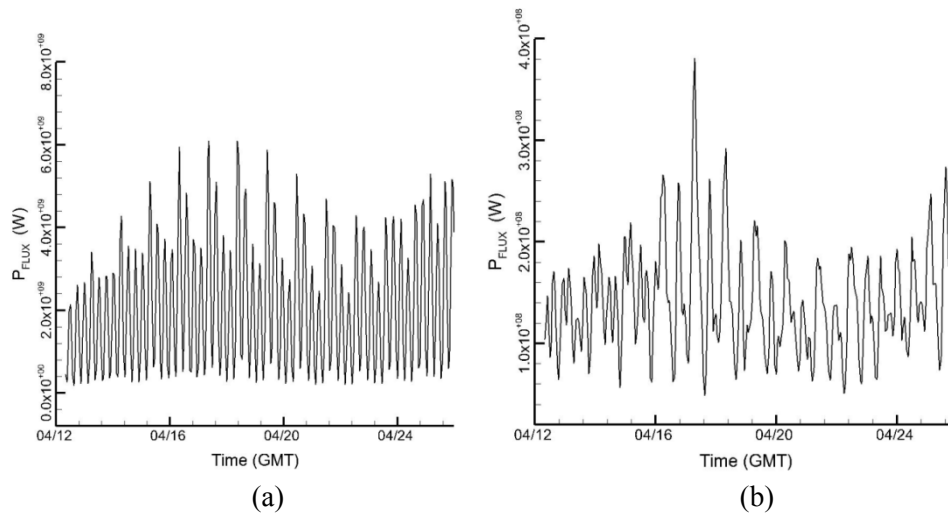


Fig. 11. Instantaneous total MHK energy flux. a) Whole MAB. b) NJ coast.

For an overall view of tidal energy along NJ coastlines, the 14-day average value of tidal power density is evaluated by formula (6) and presented in Fig. 12. The figure shows that most water bodies at estuary scales in the MAB have weak MHK energy, except in Delaware Bay, at the mouths of Hudson River and Long Island Sound, and at northeastern corner of the computational domain. Nevertheless, at small spatial scales, many sites with high MHK energy are found in NJ nearshore regions, especially where constriction occurs, e.g., Fig. 12d, and land protrudes, e.g., Fig. 12e.

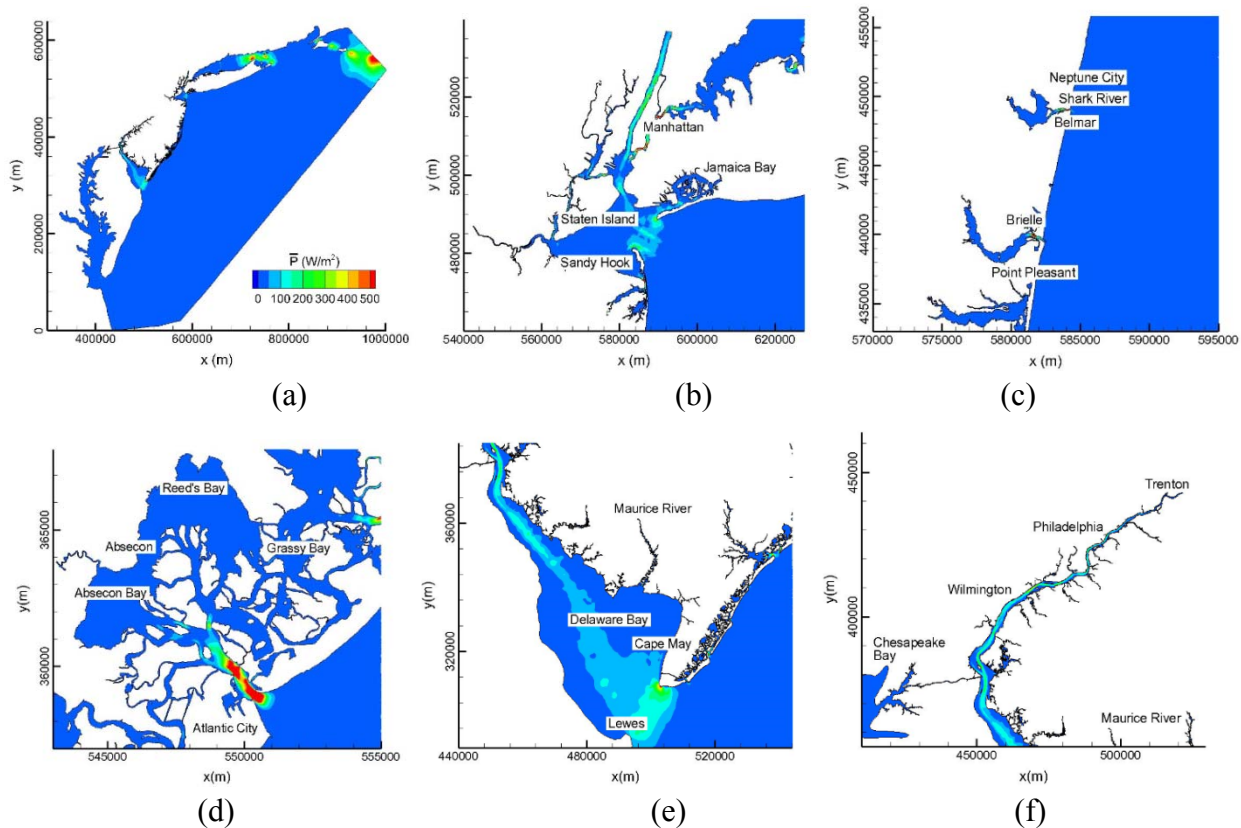


Fig. 12 Distribution of average MHK energy in the whole domain and local regions.

For a quantification of tidal energy within the whole MAB region, the average tidal power \bar{P} computed by the 2D mode on the 20 m mesh is interpolated onto an evenly spaced square grid with 361,201 nodes and spacing of 1200 m. The histogram of tidal power on these nodes is plotted in Fig. 13, which presents a tidal power spectrum from 8 W/m² to 500 W/m² that respectively correspond to 0.25 m/s and 1 m/s in magnitude of velocity. The histogram shows that, as expected, most of the regions in the MAB have small power density.

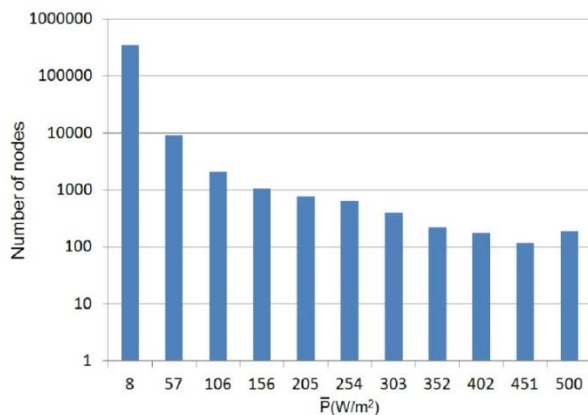


Fig. 13 Power density distribution within MAB

6.2 Location with strong tidal power density

Average power density \bar{P} is a key factor in selection of sites for power generation from MHK energy. Fig. 14 presents top locations, which are located at grid nodes, with regard to average power density at thresholds at 250, 500, 1000 W/m², which respectively correspond to 1.26, 1.59, and 2.0 m/s in peak velocity V_p , and respectively 0.63, 0.80, and 1 m/s in mean velocity V_m . In this figure, each grid node is represented by a circular dot with color corresponding to its tidal power. It is seen that there are many sites with tidal power at 250 W/m² or higher at NJ seashore (Fig. 14a). At threshold of 500 W/m² or above, still there are a lot of them, especially along the coastlines facing the Atlantic Ocean (Fig. 14b). However, only a few sites have power density at 1000 W/m² or a higher value along NJ coastlines (Fig. 14c). It is also seen that MHK energy is rich at a few locations other than NJ coasts such as Eastern River and the Long Island Sound. It should be noted that, in Fig. 14, a dot may actually represent a few grid nodes when they are very close to and cannot distinct from each other at the scale of the figure. Detailed information on power density and these sites can be viewed in the Google Earth file described as follows.

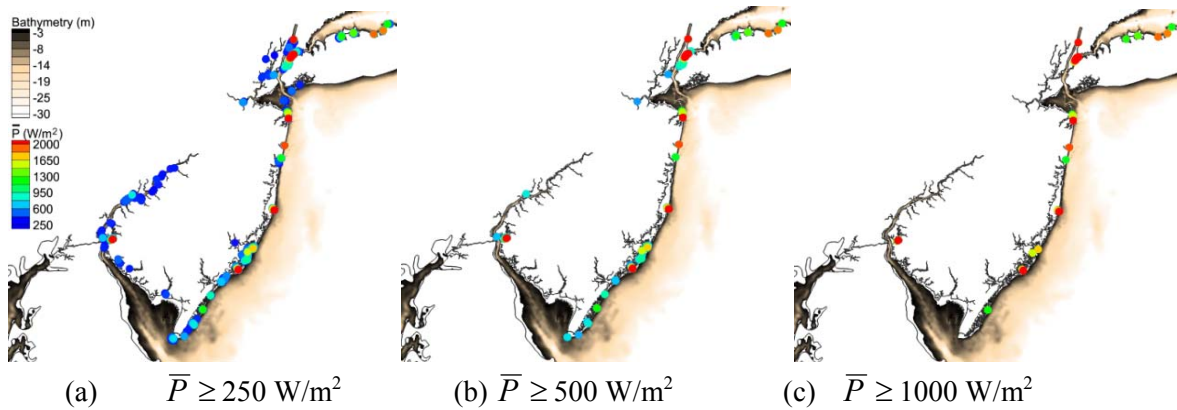


Fig. 14 Top sites with regard to average power density.

6.3 Google Earth file implemented with tidal power density

The computed distribution of average power density, \bar{P} , which is implemented as a Tecplot file, is incorporated onto a Google Earth file (Fig. 15a). Environmentally sensitive zones, locations of bridges, and other information such as the suggested location in another study of this project in [3] are also marked in the Google Earth file (Fig. 15c). With the Google Earth file, one can very conveniently view tidal power at every corner by zooming in at a point of interest (Figs. 15b, 15c, and 15d), and use it as a powerful tool for analysis of MHK energy and identification of top sites for tidal power generation.

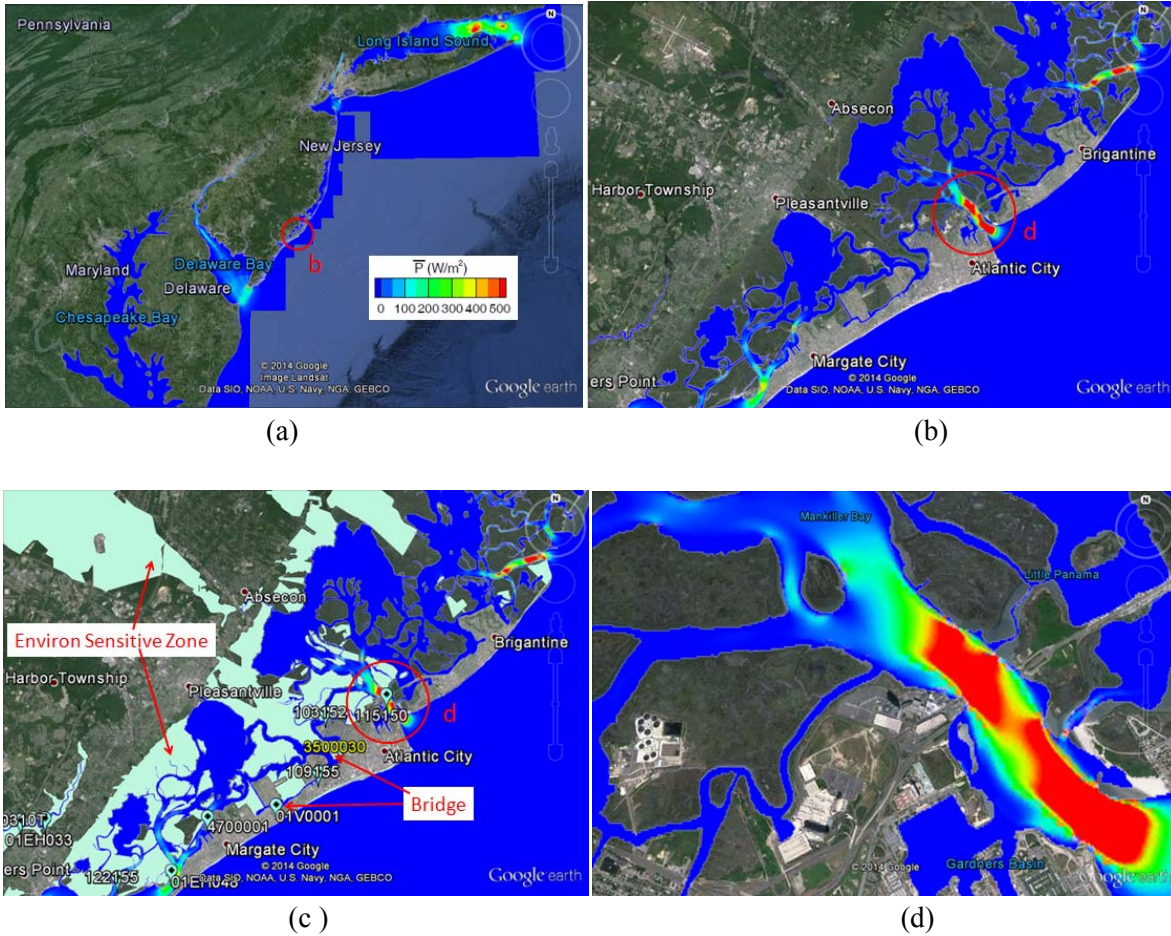


Fig. 15 The Google Earth file for distribution of tidal power. (a) An overall view. (b) A zoom view at b marked in (a). (c) Same as (b), but with environmentally sensitive zones, the shadow regions, and locations of bridges turned on. (d) A zoom view at d in (b) and (c).

7. Top Sites for Tidal Power

The potential sites for tidal power generation should be selected according to parameters including strength of tidal energy, surface area, and water depth. As a main restriction on tidal power generation, environmental impact is desired to be kept at a low and acceptable level, and development of tidal power is prohibitive in an environmentally sensitive zone. In addition, restriction will come from power generation equipments. Usually, there is a cut in velocity for tidal power generators, which range from 0.5 m/s to 1 m/s depending on their design [56,57]. In view of the need for tidal power from low speed currents and cut in velocity of power the equipments, a threshold value of 250 W/m² in averaged tidal power density \bar{P} is used, which corresponds to 1.26 m/s in peak velocity and is also used in other investigations [58]. Water surface area and depth

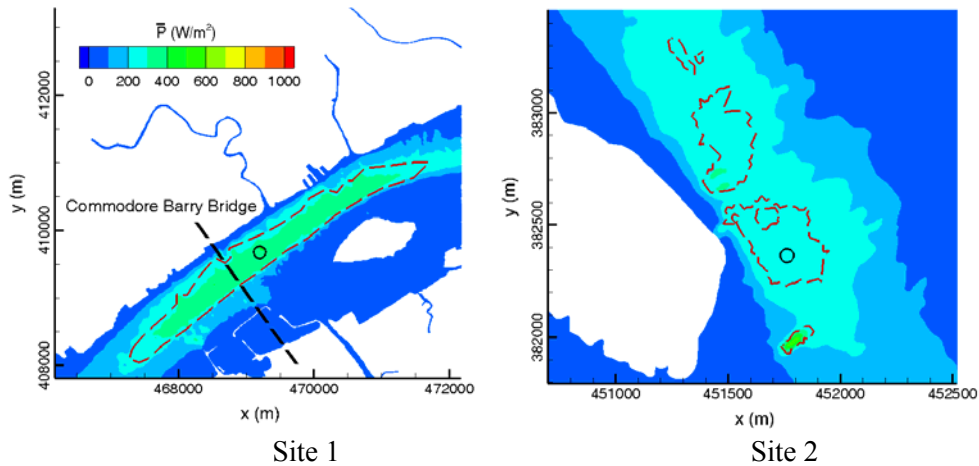
desired for a potential site for tidal power are related to spatial scales of power generation facilities, which are in general in $O(10)$ m, and requirements for their installation [26]. The power generators for low speed currents are $O(1)$ m in spatial scales, and they can be even smaller if micro-hydrokinetic technology is used [59,60].

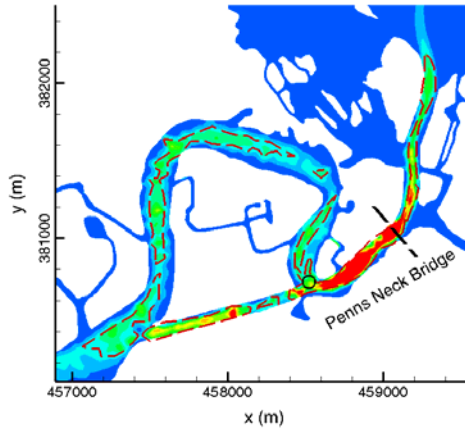
Actually, consideration of more factors is desired, such as geotechnical information that is necessary for installation of foundation structures to which the power generation facilities are attached [54], but they are not within the scope of this project and will not be considered.

In view of the above discussion, in this project, the following criteria are used to pick up top zones along the entire computational domain:

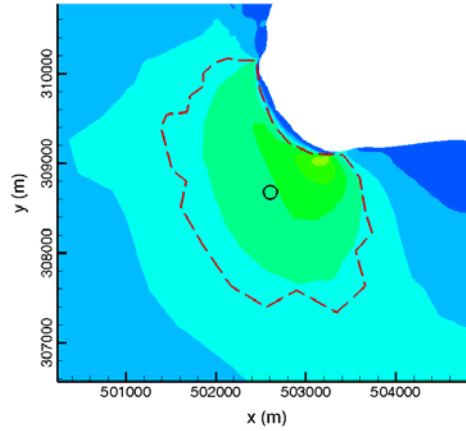
1. $\bar{P} > 250 \text{ W/m}^2$
2. Minimum horizontal scale of surface area $> 50 \text{ m}$
3. Water depth $> 2 \text{ m}$

According to the criteria, on the map of distribution of \bar{P} in Fig. 15a, all regions with $\bar{P} < 250 \text{ W/m}^2$ are blanked out, and thus only zones with $\bar{P} > 250 \text{ W/m}^2$ will remain. Furthermore, the left zones are filtered by removing zones with minimum surface width less than 50 m as well as those with depth less than 2 m. Consequently, the final tidal power zones left on the map are those meet the listed criteria and are potential locations to extract tidal energy. 31 sites with the desired tidal power zones are found as shown in Fig. 16. In this figure, such final zones are enclosed by dashed lines in red. It is seen that such zones of a site can be in forms of a single patch, e.g., Site 2 and 3, and multiple patches, e.g., Site 1 and 4. It should be noted that many spots with high values in power density marked in Fig. 14 may not show up within a potential site for tidal power as they are not associated with a surface area enough large, or, a water body enough deep.

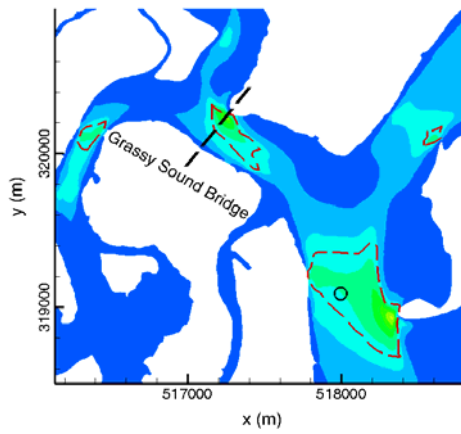




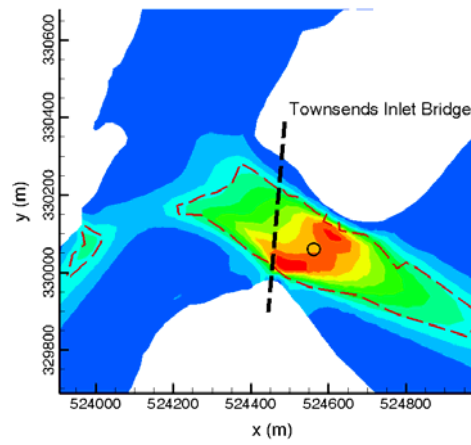
Site 3



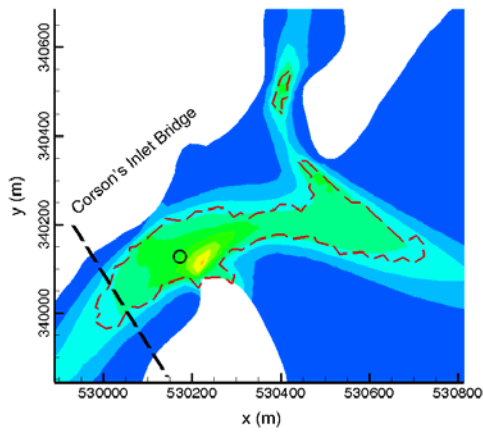
Site 4



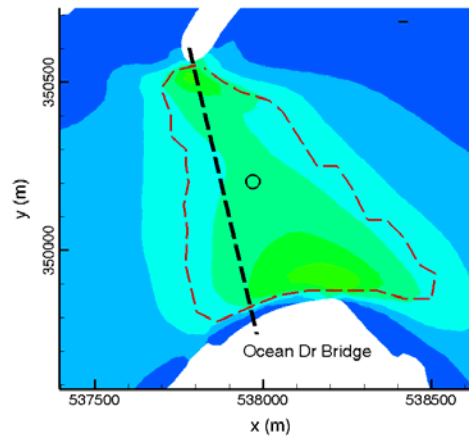
Site 5



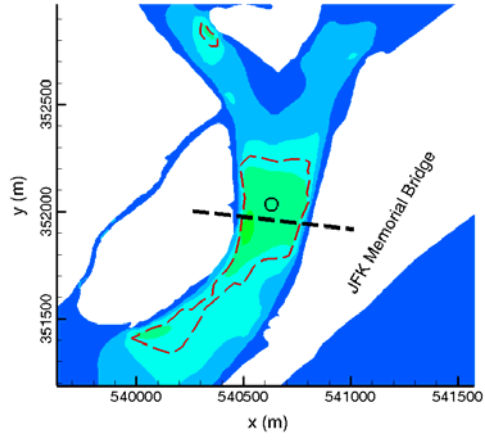
Site 6



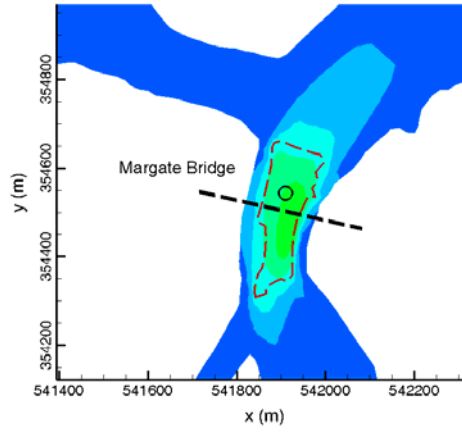
Site 7



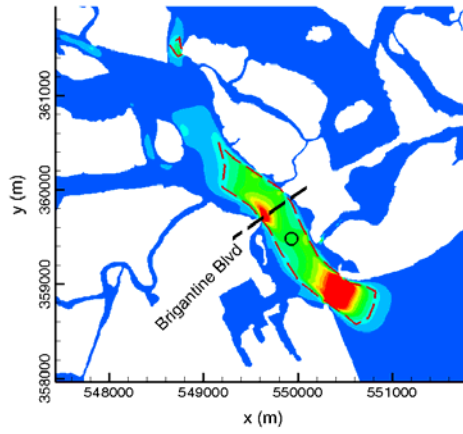
Site 8



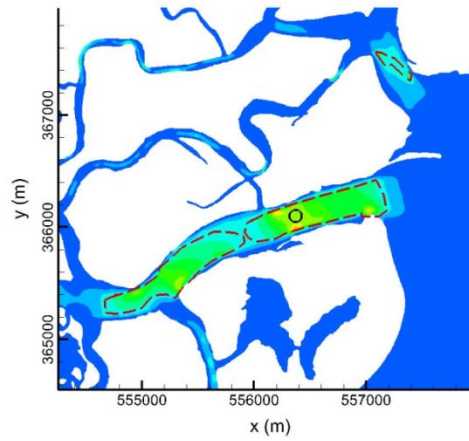
Site 9



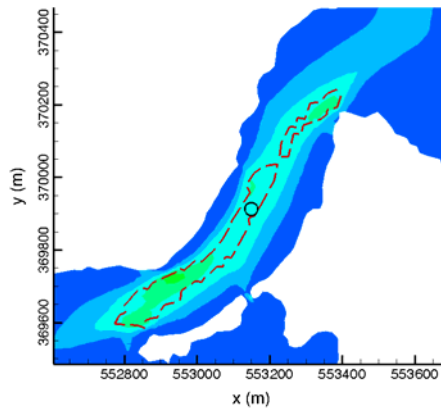
Site 10



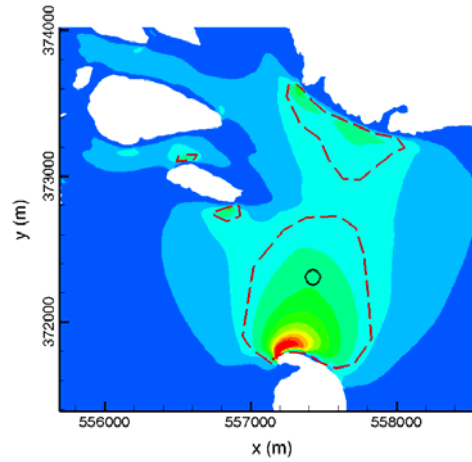
Site 11



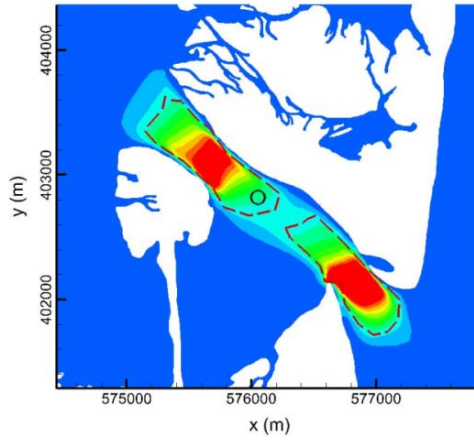
Site 12



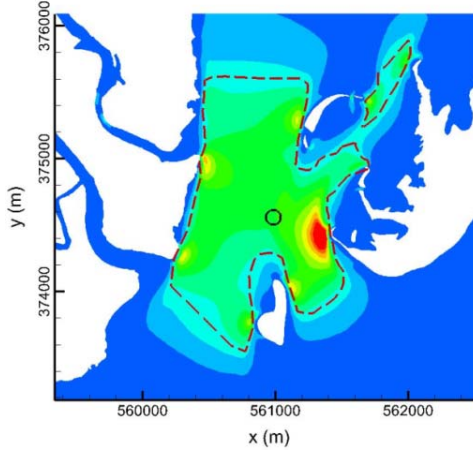
Site 13



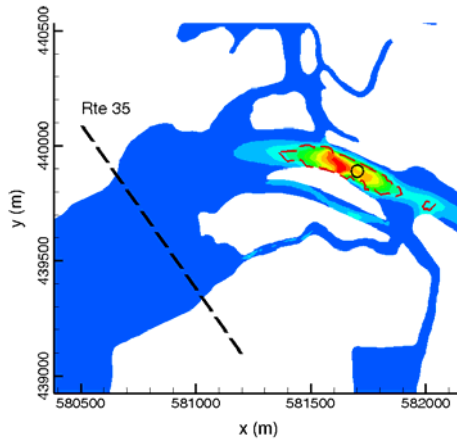
Site 14



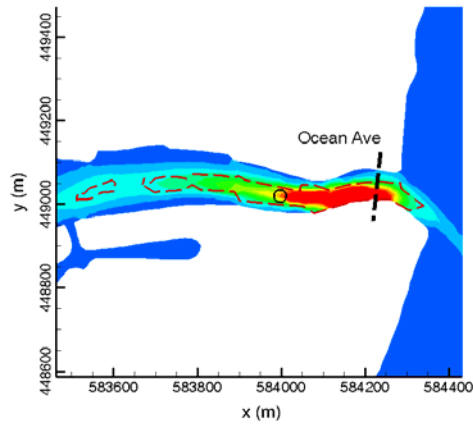
Site 15



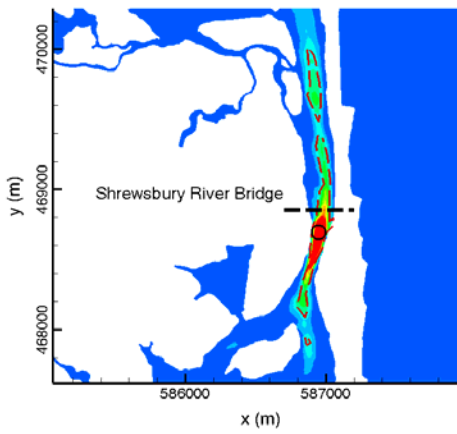
Site 16



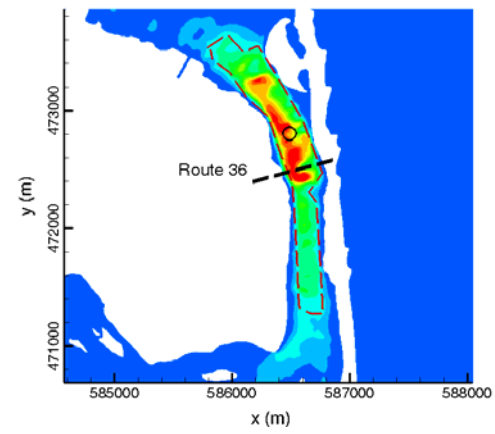
Site 17



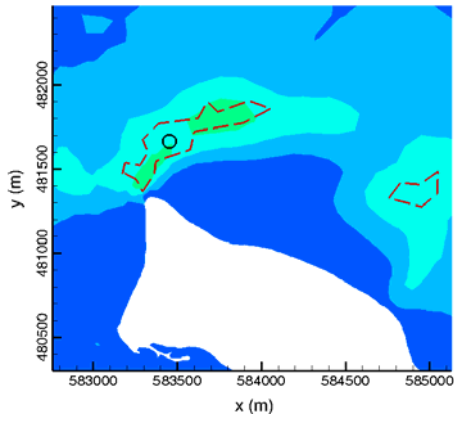
Site 18



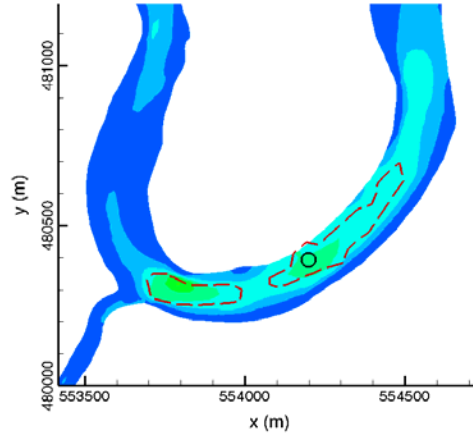
Site 19



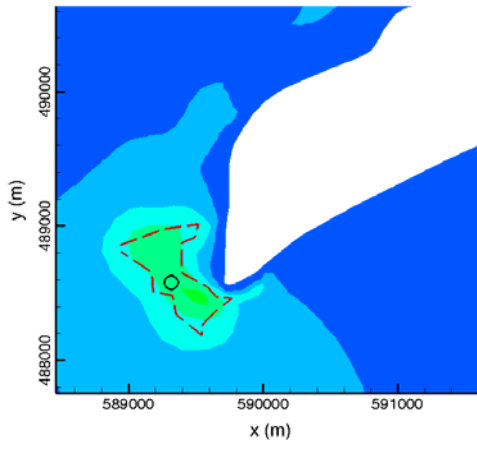
Site 20



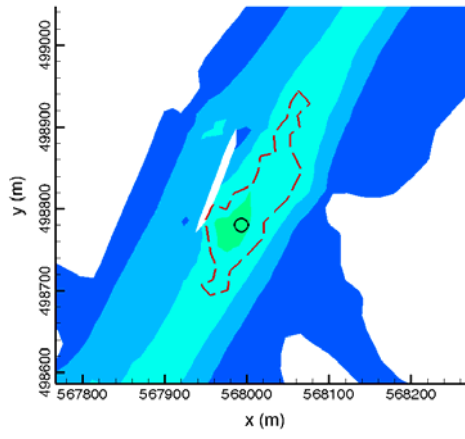
Site 21



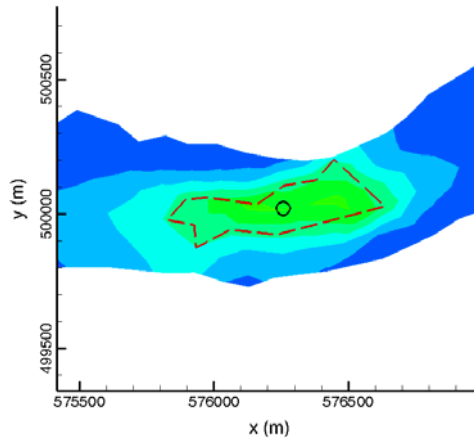
Site 22



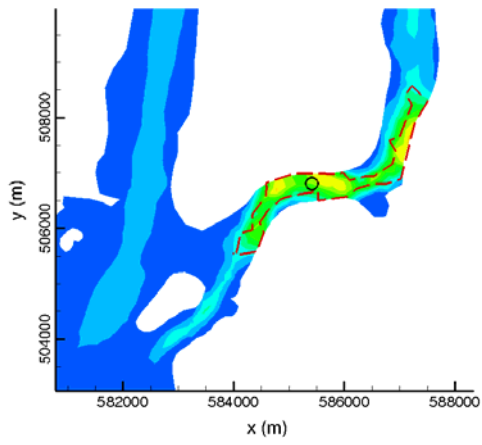
Site 23



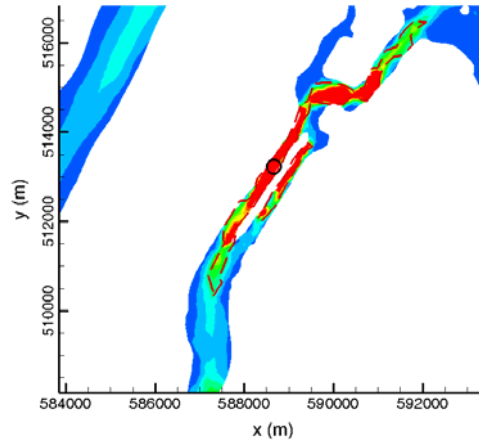
Site 24



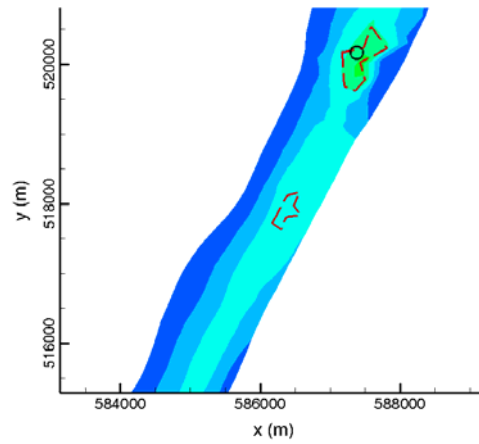
Site 25



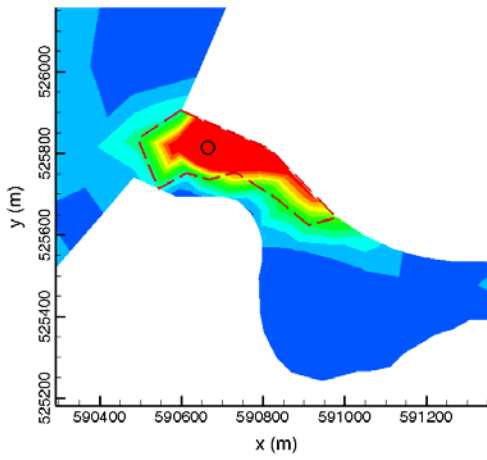
Site 26



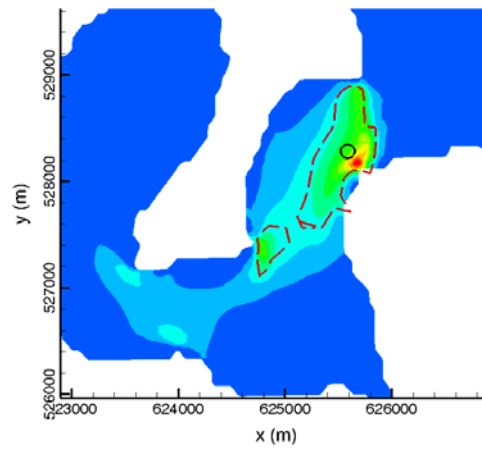
Site 27



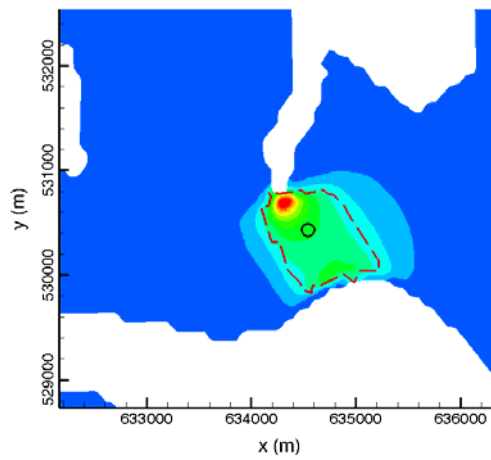
Site 28



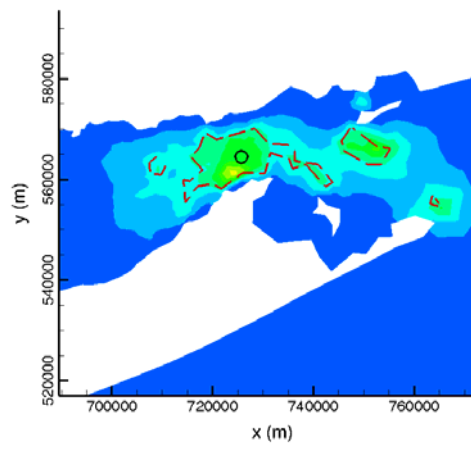
Site 29



Site 30



Site 31



Site 32

Fig. 16 Potential sites for tidal power. Dashed lines in red are the boundaries for identified tidal power zones, the dashed lines in black, e.g., that at Site 1 indicate locations of bridges, and the circles mark the locations whose latitude and longitude represent the locations of the local sites.

In order to determine the surface area of the identified power zones at a site, first, on the map of tidal energy distribution in Fig. 4a, only zones that satisfy above criteria are kept and all others are blanked out (Fig. 17a). Then, grids with square cells are used to cover the left zones (Fig. 17b), and the total number of cells that cover them is counted to estimate the area of the identified zones that meet the criteria listed above.

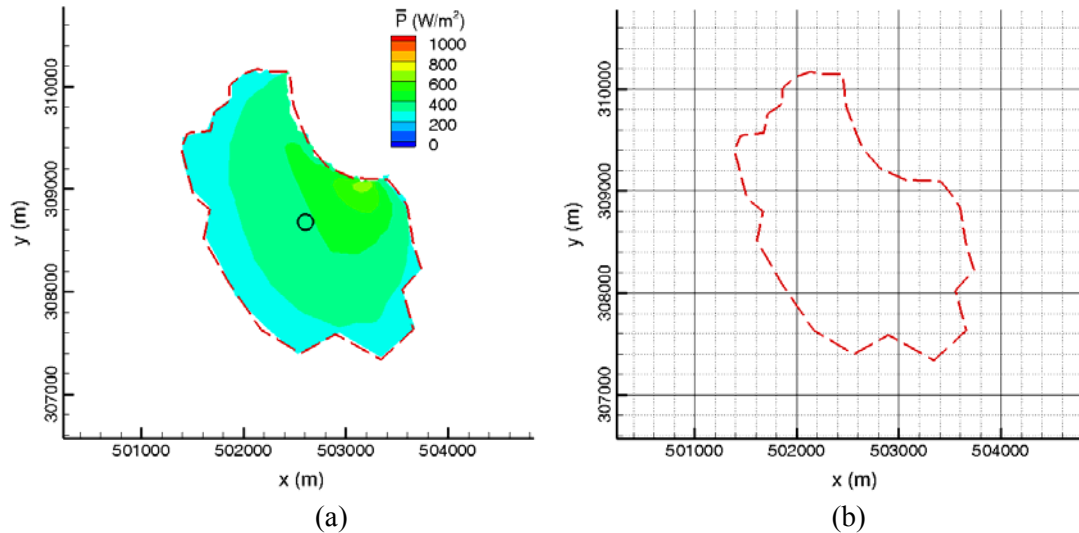


Fig. 17 Computation of surface area of the tidal power zone, at Site 4 in Fig. 16. (a) Identification of the tidal power zone. (b) Division of the zone by a grid to compute its area.

All identified sites, together with their names, locations, power density, areas, depth, and information of whether next environmentally sensitive zones, are listed in Table 5. There are totally 32 sites, with 21 along NJ coastlines and another 10 sites at NY coast. In view of the high-resolution modeling at the entire NJ coast, it is expected that those listed sites include all of its potential ones for consideration of tidal power generation. Since the mesh resolution is relatively coarse at NY coast, the sites there and the associated computed values may not be as accurate as those at the NJ coast. As illustrated in Fig.18, most potential sites for power generation are located at the east side of NJ coast facing the Atlantic Ocean. The 21 identified sites in NJ include those suggested by the sub-contractor of this project [30]. In addition, two sites are identified in East River, e.g., Site 26 and 27, and both of them have a fairly large area. In particular, the modeling captured Site 27 as a site with strong power density. Although the computational mesh is not fine within the East River, the computed values for power density and peak velocity compare reasonably with measurement there [61]. Actually, this site hosts the Verdant Power's RITE project.

Table 5 Potential sites for tidal power

No.#	Name	Location (lat.,lon.)	Power density (W/m ²)	Area (m ²)	Depth range (m)	Distance to Environ. Zone (m)
1	Chester Island	39°50'4.66"N; 75°21'37.64"W	258.7 ~ 391.2	1764000	8.2 ~ 16.3	333
2	Pea Patch Island	39°35'34.43"N; 75°33'49.08"W	251.1 ~ 562.3	169500	5.6 ~ 17.3	1356
3	Hickory Island	39°34'32.40"N; 75°28'49.24"W	269.8 ~ 2995.6	338000	2.3 ~ 10.4	0
4	Cape May Point	38°55'46.30"N; 74°58'23.77"W	261.9 ~ 589.4	3816000	4.0 ~ 7.7	0
5	Anglesea	39° 1'16.55"N; 74°47'35.98"W	253.9 ~ 624.8	291000	2.0 ~ 2.9	0
6	Townsend's Inlet	39° 7'3.70"N; 74°42'52.96"W	284.3 ~ 1035.9	110375	2.8 ~ 3.3	482
7	Corson Inlet	39°12'18.89"N; 74°39'12.94"W	293.2 ~ 456.2	75200	2.7 ~ 3.9	137
8	Great Egg Harbor Inlet	39°18'6.51"N; 74°33'24.25"W	268.7 ~ 565.1	319000	2.5 ~ 3.3	377
9	Longport	39°18'54.21"N; 74°31'45.11"W	252.4 ~ 439.2	181000	2.0 ~ 2.6	0
10	Bayshore Lagoon	39°20'14.93"N; 74°30'49.89"W	279.6 ~ 467.5	26440	2.0 ~ 2.9	0
11	Absecon Inlet	39°22'58.49"N; 74°25'15.15"W	315.1 ~ 2047.6	708000	2.0 ~ 2.0	0
12	Elder Island	39°26'32.67"N; 74°20'28.66"W	266.4 ~ 713.9	585000	2.0 ~ 2.0	0
13	Hammock Cove	39°28'41.45"N; 74°22'52.91"W	253.4 ~ 446.2	34380	2.0 ~ 2.0	1559
14	Little Egg Inlet	39°30'5.15"N; 74°19'24.32"W	257.4 ~ 1096.1	895000	2.0 ~ 2.4	1160
15	Tucker Island	39°30'40.16"N; 74°17'56.82"W	270.2 ~ 1270.1	1718000	2 ~ 2.2	262
16	Barnegat Light	39°46'20.35"N; 74° 6'55.87"W	289.1 ~ 2546.3	682000	2 ~ 2.3	2554
17	Sedge Island	40° 6'23.29"N; 74° 2'46.09"W	280.8 ~ 1041.7	38400	2.1 ~ 4.4	0
18	Shark River Inlet	40°11'14.19"N; 74° 0'46.35"W	261.1 ~ 1757.1	26625	2.5 ~ 3.9	0
19	Sea Bright	40°21'49.97"N; 73°58'33.34"W	273.4 ~ 2263.0	117000	2.8 ~ 5.9	0
20	Highlands	40°23'58.42"N; 73°58'47.64"W	267.6 ~ 1137.5	562000	2.0 ~ 6.3	0
21	Sandy Hook	40°29'5.26"N; 74° 0'4.92"W	274.4 ~ 373.4	140000	5.7 ~ 19.4	653
22	Sayreville	40°28'16.04"N; 74°21'48.26"W	267.2 ~ 489.4	53250	2.0 ~ 2.0	New York region
23	Breezy Point Tip	40°32'43.57"N; 73°56'40.13"W	287.2 ~ 427.3	242500	5.1 ~ 7.7	New York region
24	Goethals Bridge	40°38'11.32"N; 74°11'45.63"W	250.7 ~ 328.9	9670	12.7 ~ 13.1	New York region
25	New Brighton	40°38'51.43"N; 74° 5'41.87"W	308.3 ~ 524.7	100125	2.7 ~ 5.6	New York region
26	Manhattan Bridge	40°42'24.93"N; 73°59'23.70"W	264.2 ~ 782.9	1372000	8.5 ~ 17.4	New York region
27	Roosevelt Island	40°45'50.63"N; 73°56'59.08"W	275.4 ~ 5379.5	1727000	6.4 ~ 22.5	New York region
28	Hudson River	40°49'37.12"N; 73°57'48.63"W	250.5 ~ 435.3	273000	9.1 ~ 16.1	New York region
29	Henry Hud Pkwy(Toll road)	40°52'40.70"N; 73°55'23.18"W	251.9 ~ 1975.7	48160	3.3 ~ 12.8	New York region
30	Centre Island	40°53'41.17"N; 73°30'34.69"W	269.5 ~ 1112.9	538000	2.0 ~ 2.1	New York region
31	Sand City Island	40°54'43.12"N; 73°24'11.91"W	275.3 ~ 1126.5	677000	2.0 ~ 2.3	New York region
32	Essex	41°12'17.18"N; 72°17'34.26"W	257.8 ~ 736.0	195000000	14.1 ~ 53.7	New York region

Note: Sites with depth of 2 m need further examination because of lack of bathymetry data.



Fig. 18 Locations of potential sites for tidal power generation.

The tidal power resource is indeed rich at the coast; as seen in Table 5, among the 32 identified sites, there are 14 sites where power density reaches a value over 1000 W/m^2 , with 10 in NJ and 4 in NY. In addition, these sites have relatively large surface area, 210 km^2 , most of which is attributed from huge area of Site 32 at the mouth of the Long Island Sound, and that at the NJ coast is 13 km^2 . Among all of these sites, about half of them may need consideration in actual development of power generation since their depth is less than 4 m. In the computer modeling, water depth is set as 2 m at locations, mostly tributaries, where there is lack of bathymetry data. Therefore, sites with water depth of 2 m need further examination as necessary bathymetry data is available. In addition, a number of sites are next to environmentally sensitive zones, considered as distance 0 m in Table 5, and this should be taken into consideration for tidal power generation. Fig. 19 illustrates two of them. In this figure, Site 9 is next to an environmentally sensitive zone at its left bank and adjacent to a residence region at its right bank, while Site 21 is far away from either of them.

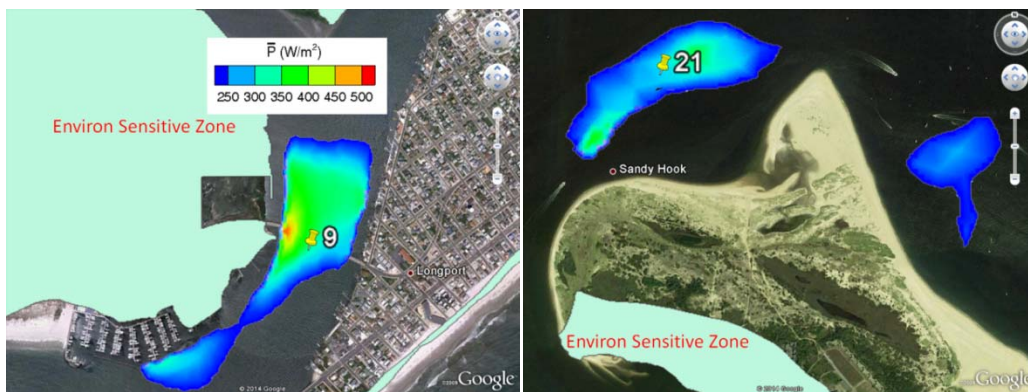


Fig. 19 Identified tidal power zones and nearby environmentally sensitive zones. (a) Site 9. (b) Site 21.

8. Top Sites for Tidal Power near Transportation Facilities

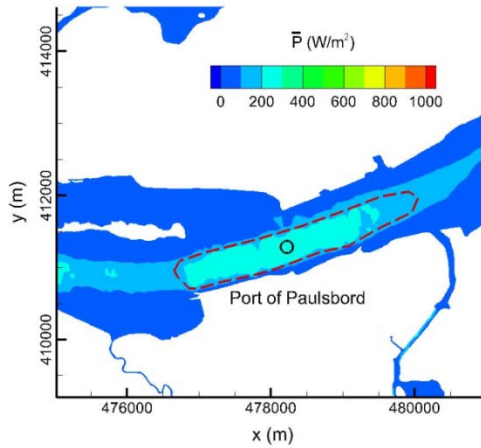
The NJ State and the NY State have a huge network of ground transportation systems such as NJ Transit, Marine Transportation System, and Metropolitan Transportation Authority, which include trains, buses, ferries, etc. This network has various infrastructures near coastlines, including bridges, docks, marinas, etc., and it will be significant to operate them using tidal power. For this purpose, a research project was initiated to make a thorough search for potential sites at NJ coast [15].

Actually, among all sites identified in the last section, many of them are next to bridges. Site 1 and 3 in Fig. 16 are two of them, at which bridges cross their tidal power zones that have a fairly large surface area with the desired value for power density. The values for power density, surface area, and water depth at the two sites can be found in Table 5, and they are favorable for power generation. In particular, power density at Site 19, can be as high as 2263 W/m^2 , which corresponds to 2.63 m/s in peak velocity V_p . Table 6 lists all of these sites and their distance to nearby bridges.

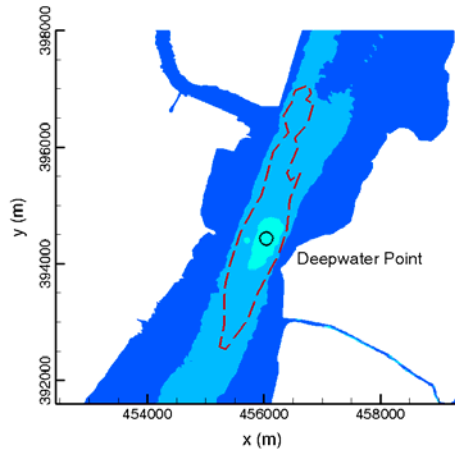
Table 6 Potential sites of tidal power near bridges

No.#	Name	Nearby bridge	Distance to bridge (m)
1	Chester Island	Commodore Barry Bridge	0
3	Hickory Island	Penns Neck Bridge	0
5	Anglesea	Grassy Sound Bridge	0
6	Townsend's Inlet	Townsend's Inlet Bridge	0
7	Corson Inlet	Corson's Inlet Bridge	0
8	Great Egg Harbor Inlet	Ocean Dr Bridge	0
9	Longport	JFK Memorial Bridge	0
10	Bayshore Lagoon	Margate Bridge	0
11	Absecon Inlet	Brigantine Blvd	0
17	Sedge Island	Rte 35	634
18	Shark River Inlet	Ocean Ave	0
19	Sea Bright	Shrewsbury River Bridge	0
20	Highlands	Route 36	0

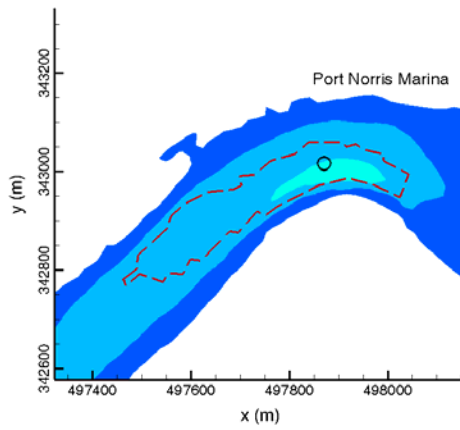
A search is also made in waters adjacent to ports, marinas, and docks at NJ coast. In general, water near these transportation facilities flows slowly, and thus their tidal energy is relatively small. Using the criteria listed previously but a threshold value of 150 W/m^2 , which corresponds to 1.06 m/s in peak velocity V_p , 10 sites have been identified, and they are shown in Fig. 20 and Table 7. It is seen that indeed tidal power is relatively small near these facilities. However, it reaches a value over 1000 W/m^2 at Site T9 and T10. In coastal waters of the NJ State and the NY State, there are many terminals for ferries between NJ and NY. Nevertheless, an examination indicates that none of them is close to a current speed at 150 W/m^2 or higher a value in tidal power.



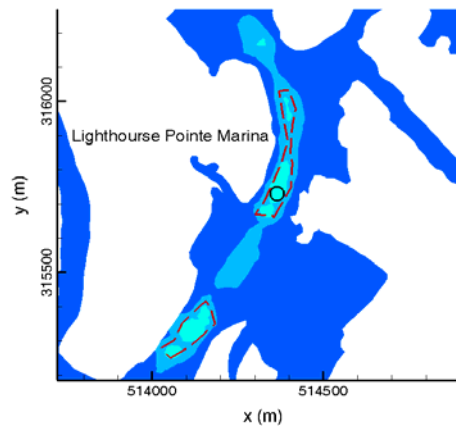
Site T1



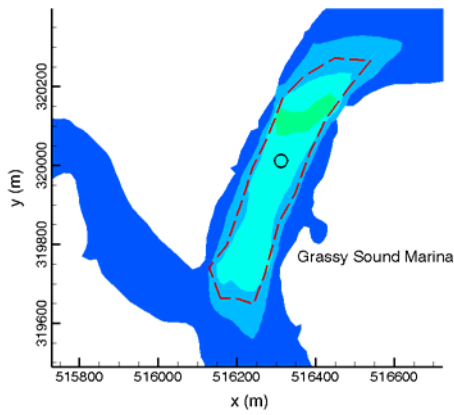
Site T2



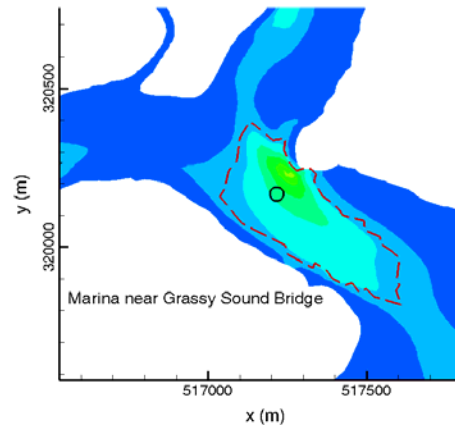
Site T3



Site T4



Site T5



Site T6

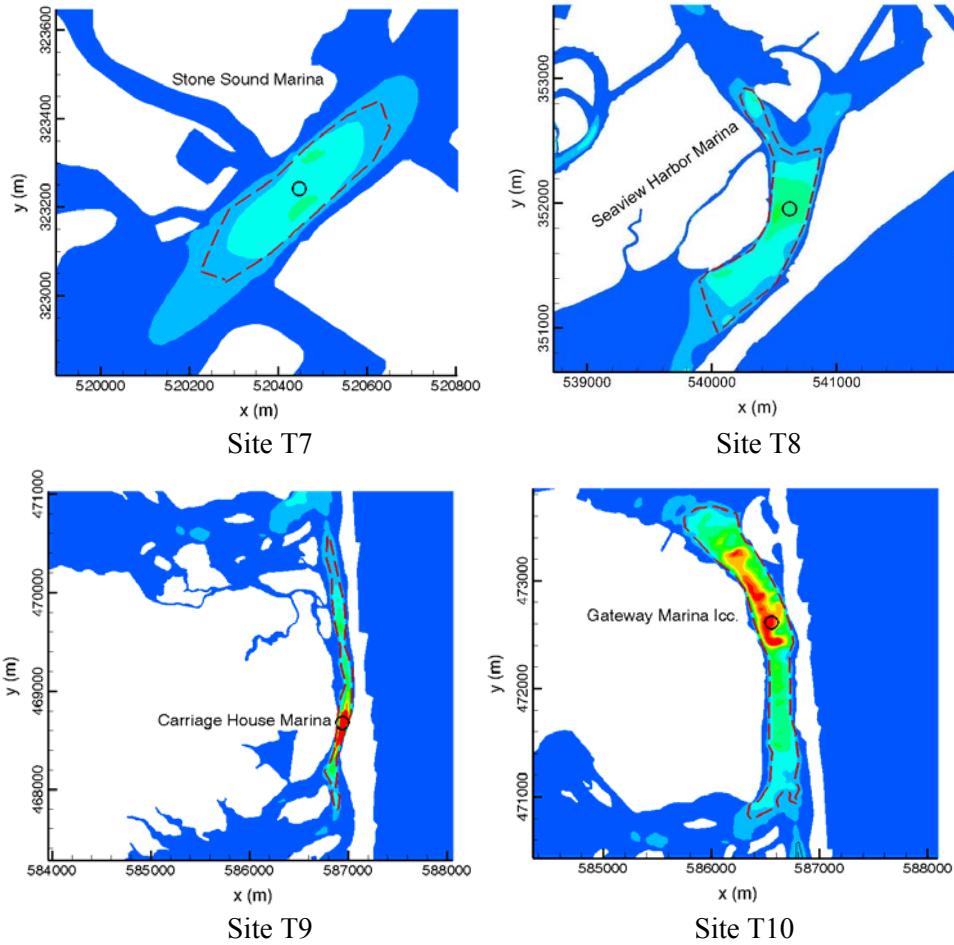


Fig. 20 Tidal power at sites near docks, marina, and ports.

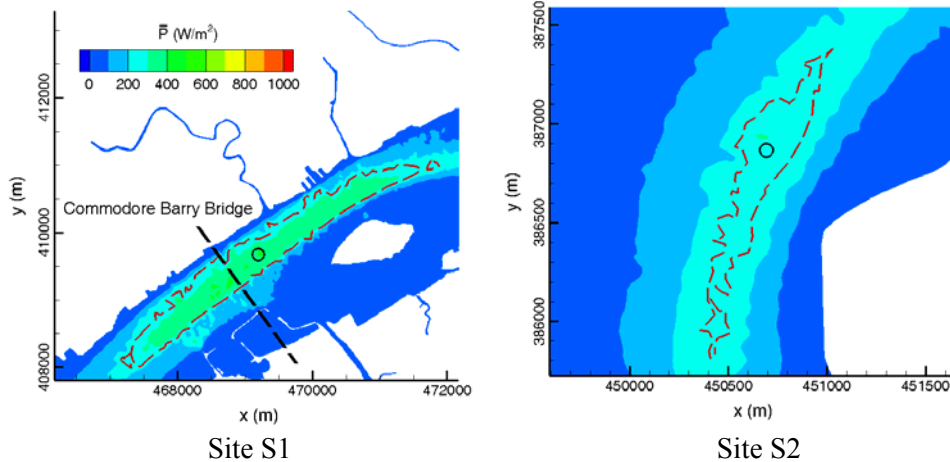
Table 7 Potential sites of tidal power adjacent to transportation facilities.

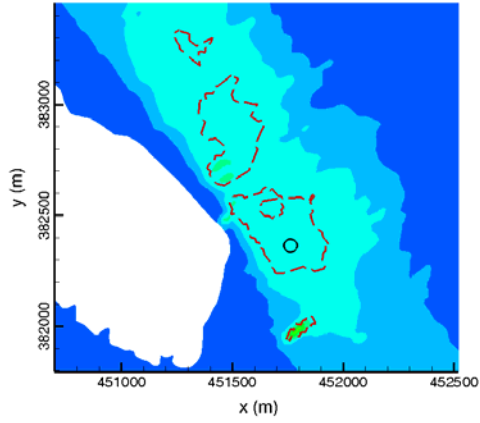
No.#	Name	Location (lat.,lon.)	Power density range(W/m ²)	Area (m ²)	Depth range (m)	Distance to Environ. Zone (m)
T1	Port of Paulsbord	39°51'6.69"N; 75°15'10.61"W	157.3-285.1	1420000	10.2-16.8	2865
T2	Deepwater point (port)	39°41'53.14"N; 75°30'40.66"W	154.1-222.4	2112000	10.7-18.2	2623
T3	Port Norris Marina	39°14'10.32"N; 75° 1'30.09"W	157.8-239.2	46320	2.0-2.0	0
T4	Lighthouse Pointe Marina	38°59'25.10"N; 74°50'2.56"W	153.7-264.1	23580	2.0-4.2	0
T5	Grassy Sound Marina	39° 1'46.95"N; 74°48'40.39"W	154.5-357.8	78030	2.0-2.0	0
T6	Marina near Grassy Sound Bridge	39° 1'49.29"N; 74°48'0.18"W	160.8-603.3	130140	2.2-2.5	0
T7	Stone Sound Marina	39° 3'28.87"N; 74°45'47.64"W	159.2-311.2	60240	3.3-3.4	0
T8	Seaview Harbor Marina	39°18'57.34"N; 74°31'43.89"W	150.5-451.6	565000	2.0-2.7	0
T9	Carriage House Marina	40°21'49.87"N; 73°58'33.09"W	159.5-2263.4	243000	2.1-6.5	0
T10	Gateway Marina lcc.	40°23'55.88"N; 73°58'46.36"W	162.6-1132.0	746000	2.0-6.4	0

9. Sea-Level-Rise Effects

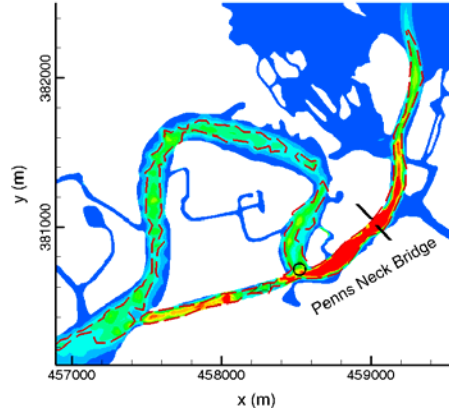
According to the computer modeling of the coastal flow under SLR of 0.5 m and its analysis [29], it is known that, in general, power density decreases around the barrier islands along the Atlantic Ocean, and it increases in the Delaware Bay and the Delaware River. But overall tidal energy at NJ seashore, in terms of the average value of the total MHK energy flux at a distance of 2 km from the coast, could increase by 21% at SLR of 0.5 m. In addition, dividing the computational domain into many small square cells and considering the histogram of tidal power within them, it is found that SLR decreases the number of cells that have $8\text{W}/\text{m}^2$ or a lower value in average power density, but in general an increase is observed for the number of cells with higher values.

Considering power density, water surface area, and water depth as described in the previous section, 32 potential sites for tidal power generation are identified as in Fig. 21 and Table 8. The table shows that, in comparison with those under current sea level condition shown in Table 5, the top sites, including those near bridges, remain the same under the SLR condition, except that two sites on the previous list disappear and two sites occurs in the new list. Nevertheless, those sites may change substantially with respect to their values in power density, water surface area, and water depth, and the patterns of the change are complicated. For instance, it is seen that in Table 8 that under the SLR condition, the value of power density at a site, in terms of its minimum and maximum, may decrease considerably, e.g., Site 6, increase noticeably, e.g., Site 19, and approximately remain the same, e.g., Site 8. This is interesting; under the SLR condition, the numbers of the sites where the tidal power density decreases, increases, and remains the same are roughly the same, although overall the tidal energy, in terms of MHK energy flux, increases at the NJ coast by 21% as indicated above. In addition, the surface area of at most sites alter substantially, it may decrease, e.g., Site 14, and may increase, e.g., Site 4, and the number of sites with an increase is roughly the same to that with a decrease in the area. Under condition of SLR of 0.5 m, it is expected that the water depth at these sites will increase roughly by 0.5 m, and indeed the Table 5 and 8 show such trend.

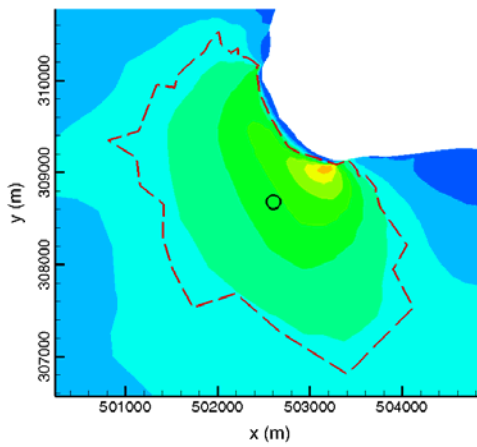




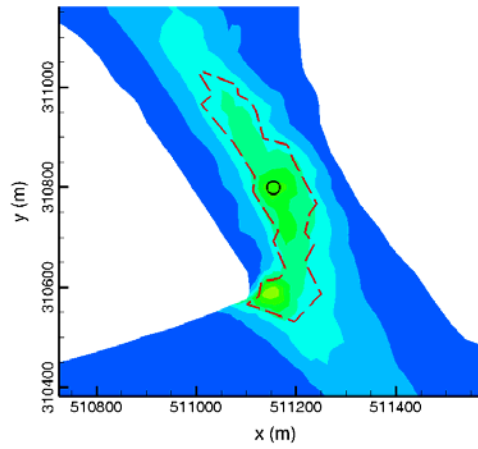
Site S3



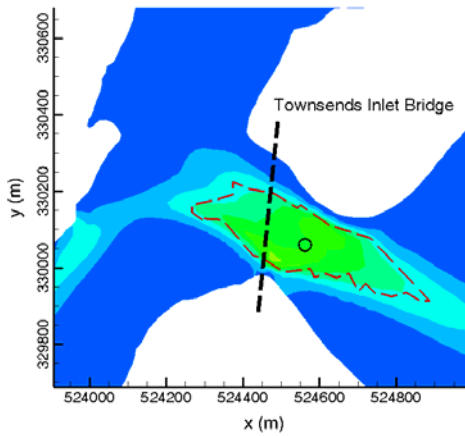
Site S4



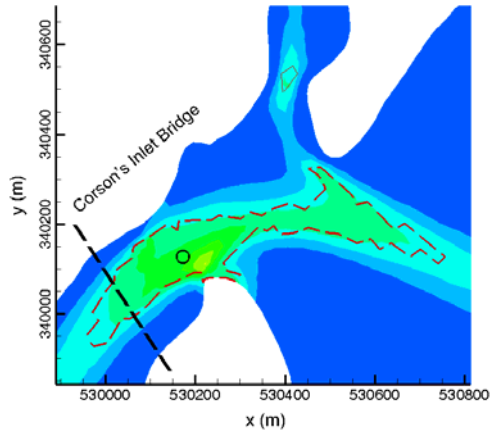
Site S5



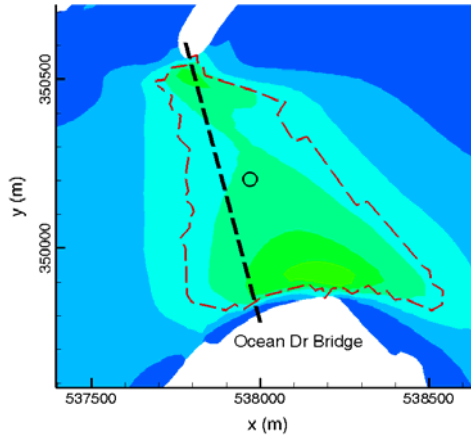
Site S6



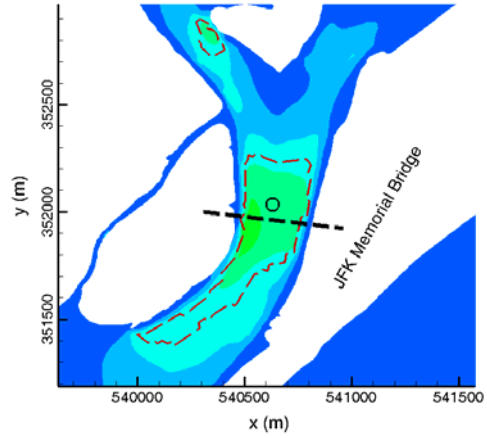
Site S7



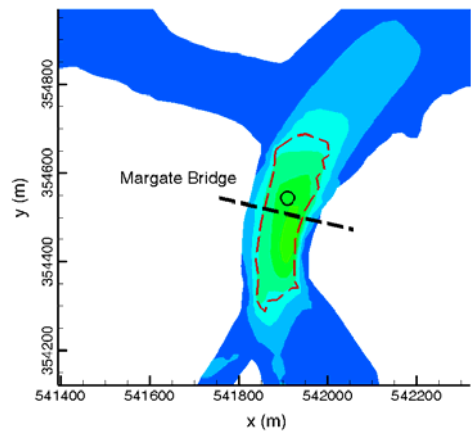
Site S8



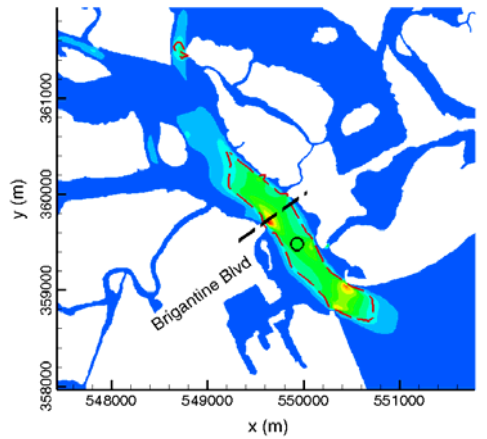
Site S9



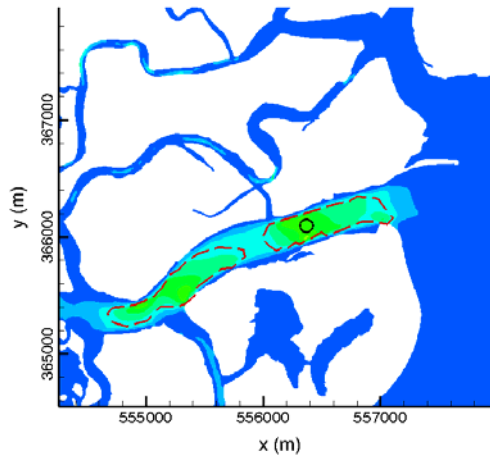
Site S10



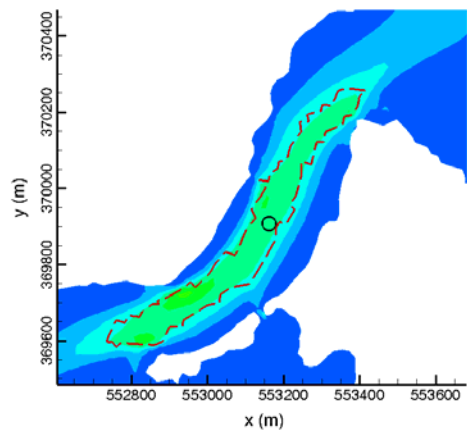
Site S11



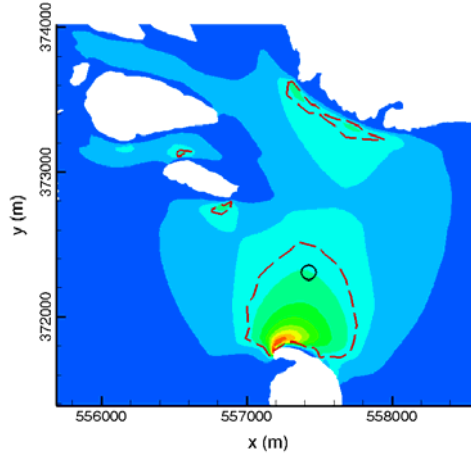
Site S12



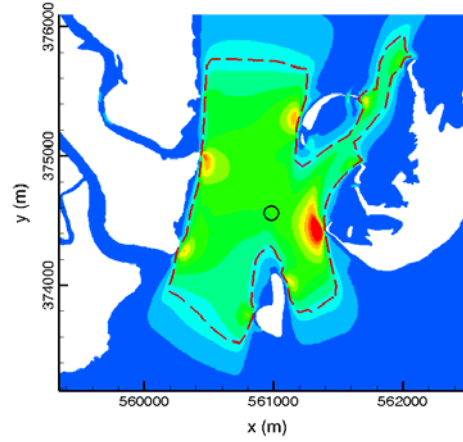
Site S13



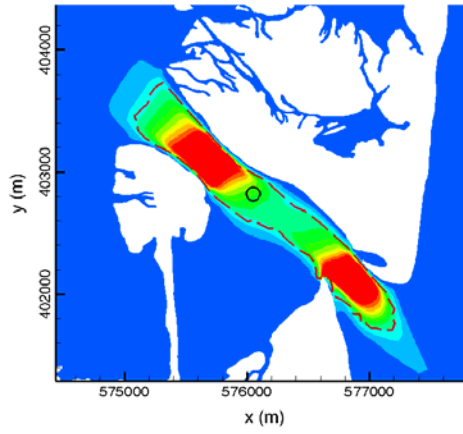
Site S14



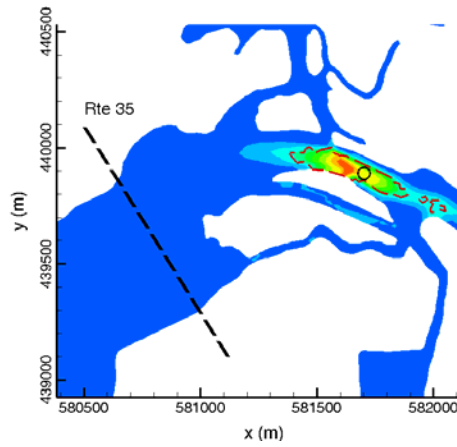
Site S15



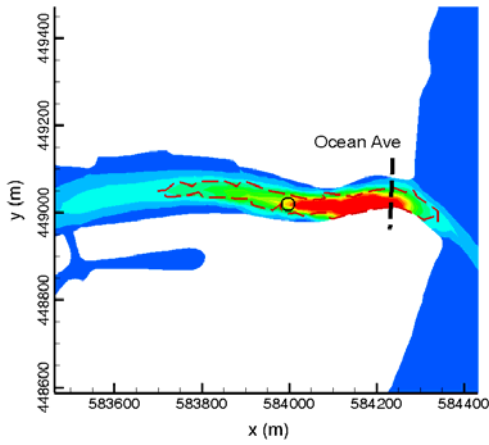
Site S16



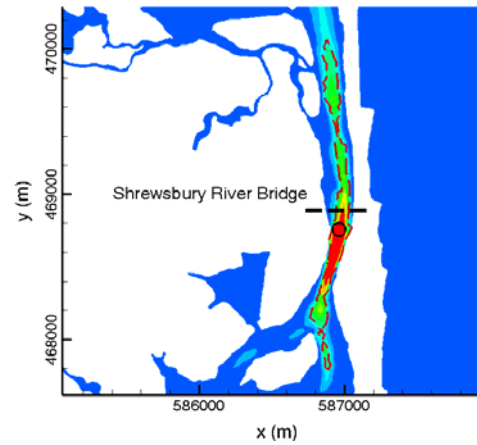
Site S17



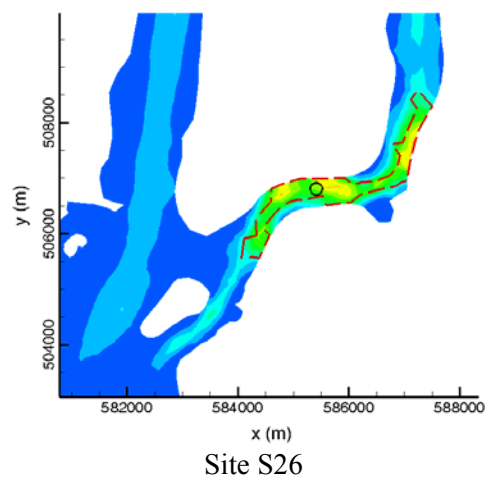
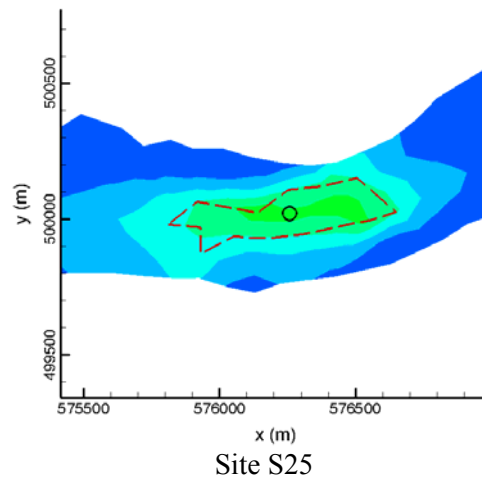
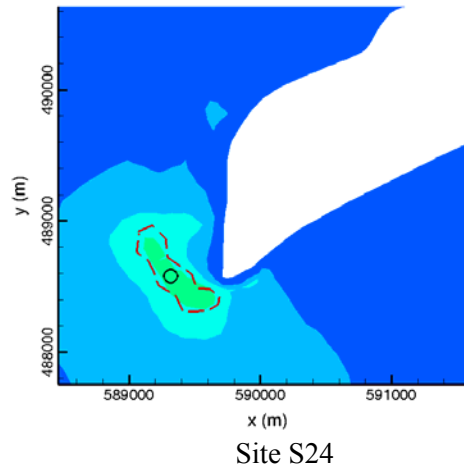
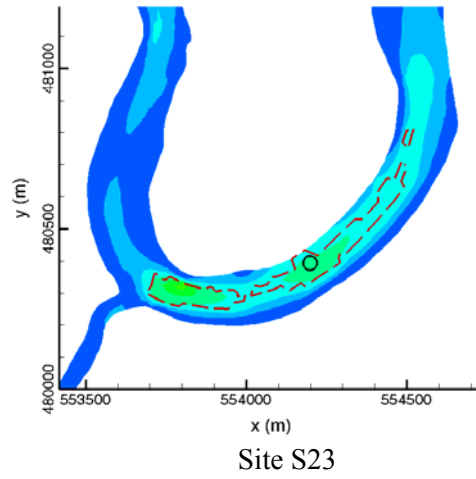
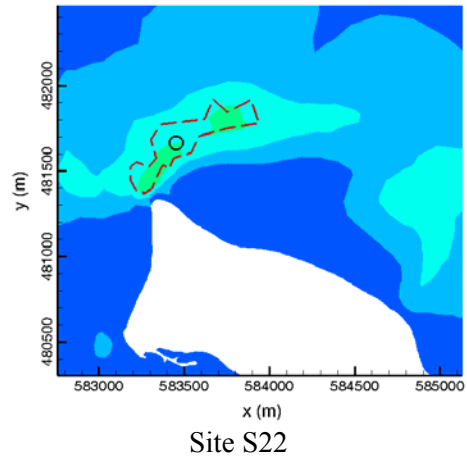
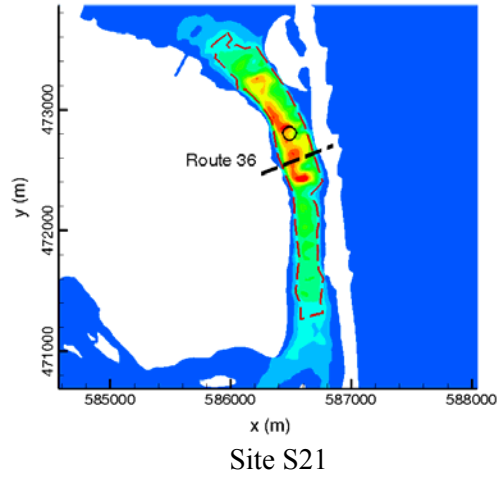
Site S18



Site S19



Site S20



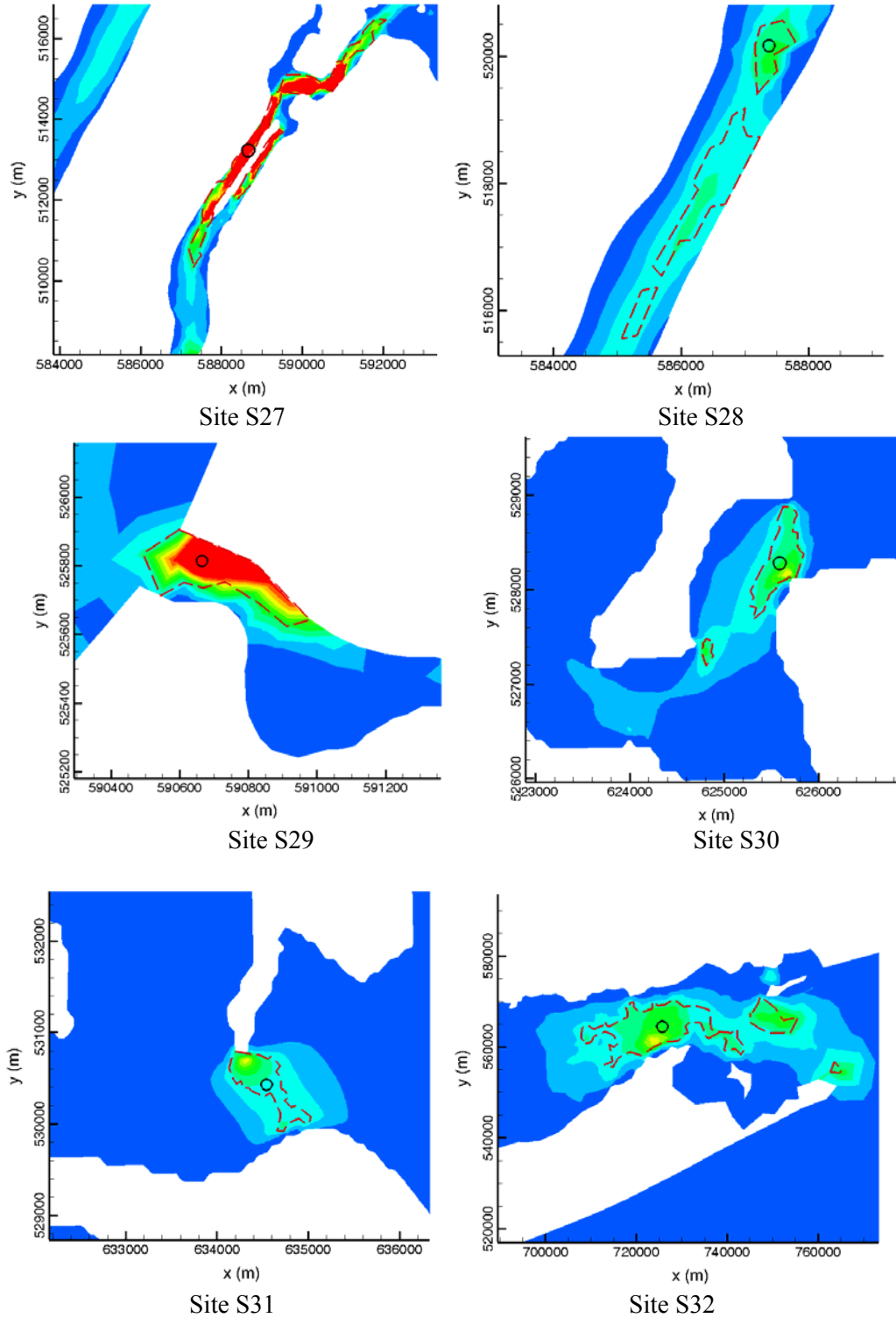


Fig. 21 Potential sites for tidal power under SLR condition.

Table 8. Potential sites for tidal power under SLR condition.

No.#	Name	Location (lat.,lon.)	Power density Range(W/m ²)	Area (m ²)	Depth range (m)	Distance to Environ. Zone (m)
S1	Chester Island	39°50'4.66"N; 75°21'37.64"W	257.7-404.9	1977600	8.8-16.8	324
S2	Pennsville Township	39°37'42.50"N; 75°34'39.43"W	250.2-300.5	192000	13.8-18.3	1199
S3	Pea Patch Island	39°35'34.43"N; 75°33'49.08"W	251.0-492.0	180750	6.75-17.7	1305
S4	Hickory Island	39°34'32.40"N; 75°28'49.24"W	267.8-3508.3	438500	2.8-12.6	0
S5	Cape May Point	38°55'46.30"N; 74°58'23.77"W	271.2-873.4	5250560	4.5-8.3	0
S6	Cape May Inlet	38°56'42.87"N; 74°52'17.90"W	259.1-671.4	38920	3.3-10.9	783
S7	Townsend's Inlet	39° 7'3.70"N; 74°42'52.96"W	273.3-627.7	71200	3.4-3.7	512
S8	Corson Inlet	39°12'18.89"N; 74°39'12.94"W	261.5-676.7	68400	3.2-4.1	140
S9	Great Egg Harbor Inlet	39°18'6.51"N; 74°33'24.25"W	263.3-565.5	316710	3.1-3.8	394
S10	Longport	39°18'54.21"N; 74°31'45.11"W	257.2-498.2	206000	2.5-3.1	0
S11	Bayshore Lagoon	39°20'14.93"N; 74°30'49.89"W	263.9-579.4	33880	2.5-3.5	0
S12	Absecon Inlet	39°22'58.49"N; 74°25'15.15"W	282.7-904.7	568800	2.5-2.5	0
S13	Elder Island	39°26'32.67"N; 74°20'28.66"W	274.7-588.3	442000	2.5-2.5	0
S14	Hammock Cove	39°28'41.45"N; 74°22'52.91"W	251.4-493.2	61740	2.5-2.5	1475
S15	Little Egg Inlet	39°30'5.15"N; 74°19'24.32"W	261.1-1000.2	474880	2.5-2.7	1130
S16	Tucker Island	39°30'40.16"N; 74°17'56.82"W	266.9-1383.4	1944000	2.5-2.7	277
S17	Barneget Light	39°46'20.35"N; 74° 6'55.87"W	276.4-2185.5	839000	2.5-3.1	2620
S18	Sedge Island	40° 6'23.29"N; 74° 2'46.09"W	284.9-969.1	37080	2.6-4.8	0
S19	Shark River Inlet	40°11'14.19"N; 74° 0'46.35"W	272.3-1626.3	22040	3.1-4.4	0
S20	Sea Bright	40°21'49.97"N; 73°58'33.34"W	283.1-2743.4	130560	2.7-6.5	0
S21	Highlands	40°23'58.42"N; 73°58'47.64"W	275.7-1126.4	536000	2.5-6.7	0
S22	Sandy Hook	40°29'5.26"N; 74° 0'4.92"W	262.9-400.7	116910	14.5-19.9	599
S23	Sayreville	40°28'16.04"N; 74°21'48.26"W	258.3-517.1	49050	2.5-2.5	New York region
S24	Breezy Point Tip	40°32'43.57"N; 73°56'40.13"W	276.1-364.2	154980	5.7-8.3	New York region
S25	New Brighton	40°38'51.43"N; 74° 5'41.87"W	286.8-446.1	101340	3.3-5.1	New York region
S26	Manhattan Bridge	40°42'24.93"N; 73°59'23.70"W	281.2-798.4	1321040	10.2-19.5	New York region
S27	Roosevelt Island	40°45'50.63"N; 73°56'59.08"W	253.6-6741.4	2427280	7.2-23.2	New York region
S28	Hudson River	40°49'37.12"N; 73°57'48.63"W	253.2-471.3	1480000	9.3-21.1	New York region
S29	Henry Hud Pkwy(Toll road)	40°52'40.70"N; 73°55'23.18"W	252.9-1773.5	48165	3.7-13.0	New York region
S30	Centre Island	40°53'41.17"N; 73°30'34.69"W	267.2-765.7	247320	2.5-2.7	New York region
S31	Sand City Island	40°54'43.12"N; 73°24'11.91"W	254.3-724.8	271750	2.5-3.2	New York region
S32	Essex	41°12'17.18"N; 72°17'34.26"W	265.1-778.5	232000000	11.9-62.5	New York region

Under the SLR condition, Site 5 and 24 in the current list disappear as a potential site for power generation, while Site S2 and S6 in the 50-year list are newly added potential sites. Fig. 22 presents tidal power at the disappearing old and newly added sites, and it illustrates how tidal power at individual sites changes with sea level. In the figure, it is seen that, the area with the desired value of power density at Site 5 in the current list shrinks almost to zero due to SLR, and that at Site S2 in the 50-year list increases to a value that sufficiently large as a potential site. Site 5 and Site S6, the former disappearing and the latter newly occurring, are next to each other, and the change of

power density at them reflects a featuring of alternation of local tidal current under the SLR condition.

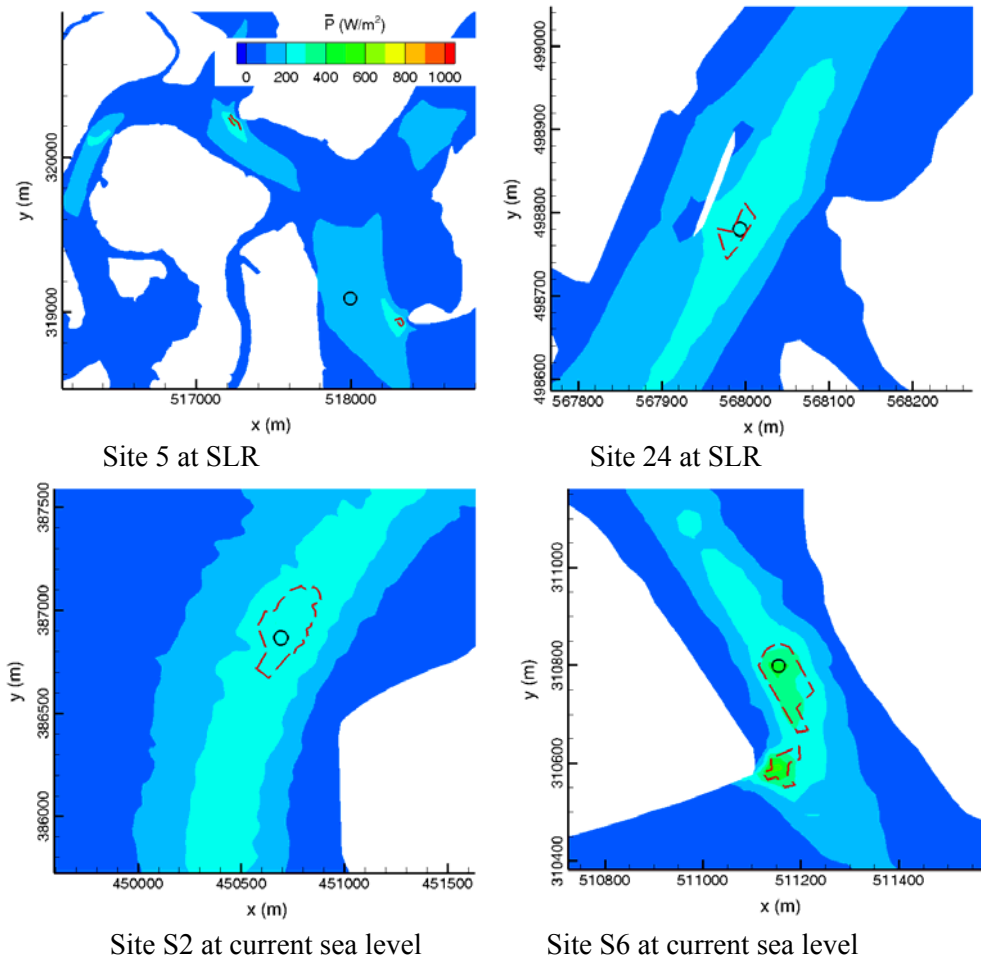
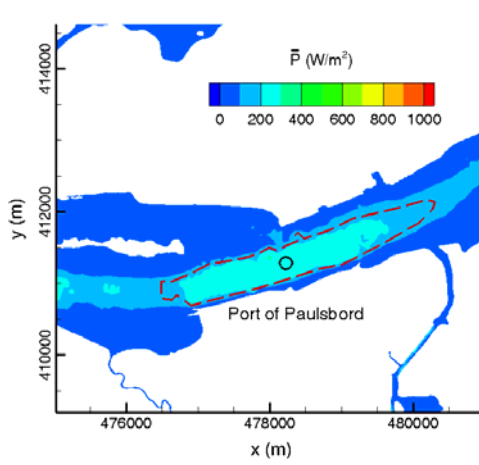
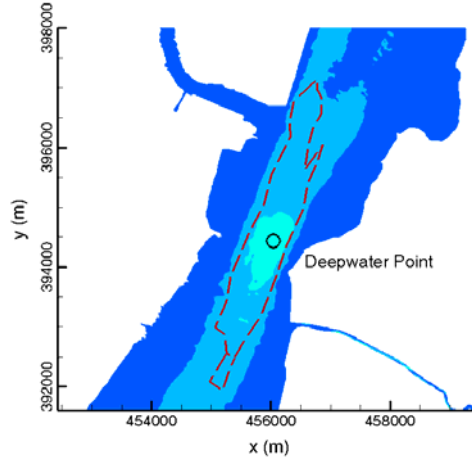


Fig. 22 Potential tidal power sites that disappear and newly occur due to SLR.

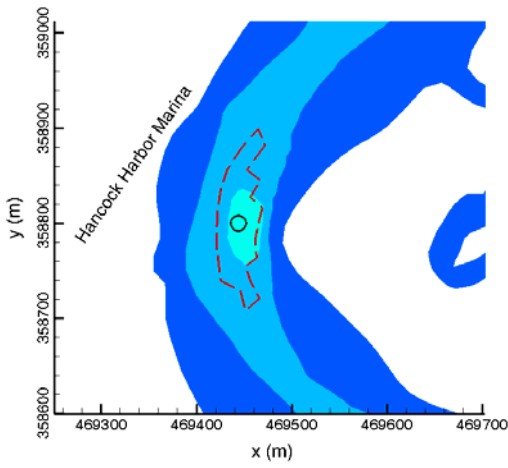
Predicted tidal power at the 10 potential sites near docks and ports listed in the previous sections is plotted in Fig. 23 and more details are listed in Table 9. It is seen that indeed tidal power is altered by SLR, however, in contrast to the discussion for the top sites in the previous section, the change of range of tidal power density at most sites, except Site 6, is rather minor. Nevertheless, the water surface areas at these sites still changes considerably, either with a decline or a growth.



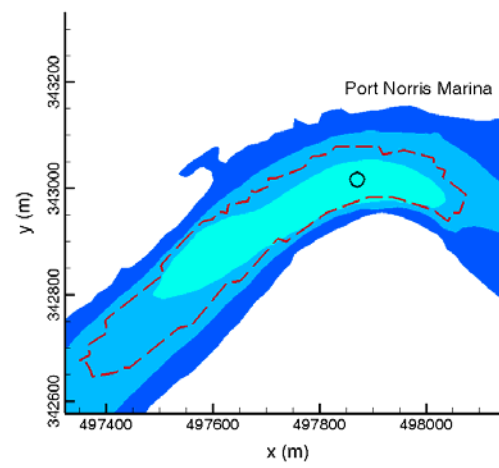
Site T1



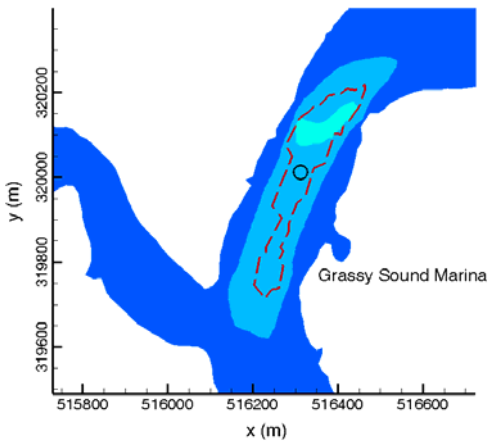
Site T2



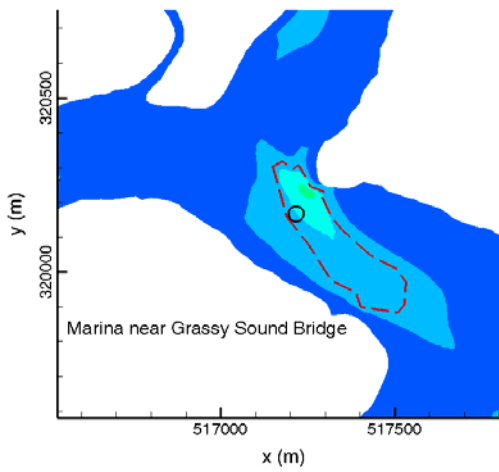
Site T3



Site T4



Site T5



Site T6

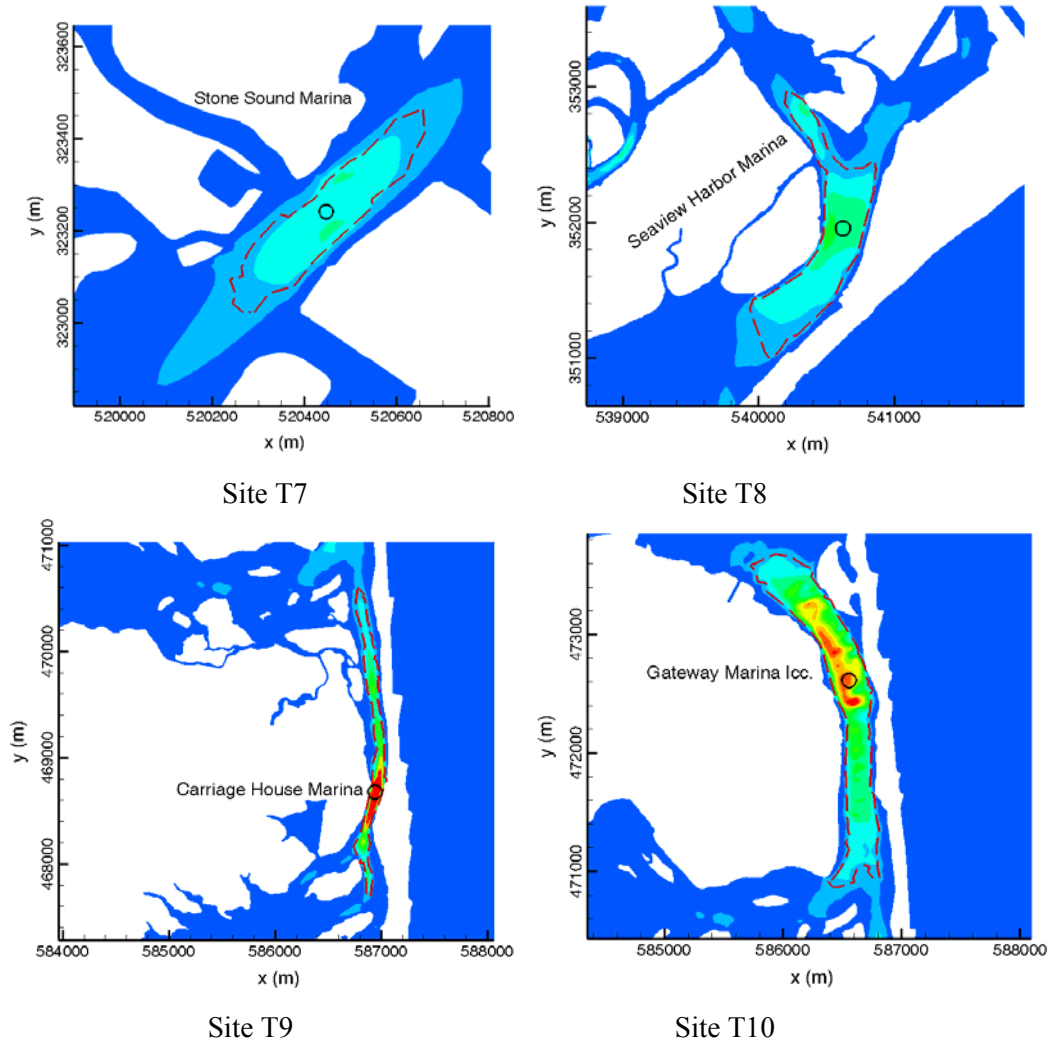


Fig. 23 Tidal power at sites near docks, marina, and ports under SLR condition.

Table 9. Potential sites for tidal power adjacent to transportation facilities under the SLR condition.

No.#	Name	Location (lat.,lon.)	Power density range (W/m ²)	Area (m ²)	Depth range (m)	Distance to Environ. Zone (m)
T1	Port of Paulsbord	39°51'6.69"N; 75°15'10.61"W	155.8-303.2	1658880	10.6-19.0	2686
T2	Deepwater point (Port)	39°41'53.14"N; 75°30'40.66"W	150.9-238.4	2624000	12.1-18.8	2466
T3	Hancock Harbor Marina	39°22'40.87"N; 75°21'16.60"W	157.7-257.9	5370	2.5-2.7	0
T4	Port Norris Marina	39°14'10.32"N; 75° 1'30.09"W	154.9-290.7	83200	2.5-2.5	0
T5	Grassy Sound Marina	39° 1'46.95"N; 74°48'40.39"W	151.6-222.9	32220	2.5-2.5	0
T6	Marina near Grassy Sound Bridge	39° 1'49.29"N; 74°48'0.18"W	153.6-322.2	56720	2.8-3.0	0
T7	Stone Sound Marina	39° 3'28.87"N; 74°45'47.64"W	157.5-308.0	53920	3.8-3.9	0

T8	Seaview Harbor Marina	39°18'57.34"N; 74°31'43.89"W	153.4-492.4	544000	2.5-3.2	0
T9	Carriage House Marina	40°21'49.87"N; 73°58'33.09"W	154.8-2754.2	265000	2.7-6.4	0
T10	Gateway Marina lcc.	40°23'55.88"N; 73°58'46.36"W	151.3-1215.0	753000	2.5-6.2	0

10. Concluding Remarks

This project makes a high-resolution modeling of coastal ocean flows at NJ and its neighbor states, and it presents an analysis of tidal energy distribution. On this basis, it provides a top list for potential sites, with emphasis on those at NJ coast, for tidal power generation considering tidal power strength, water surface area, water depth, and environmentally sensitive zones. The results show that there are 31 sites with favorable parameters for tidal power generation. Among them, 21 sites with total surface area of 13 km² are at coastlines of NJ, and many are near coastal bridges. In addition, 10 favorable sites for tidal power near transportation infrastructures in NJ are also identified. However, a number of the sites at NJ coast are located near environmentally sensitive zones and thus need further examination. In addition, SLR could substantially affect tidal energy distribution at the identified sites, and it is a factor that has to be taken into consideration in actual tidal power generation. This research is the first thorough search for tidal power sites at a fairly large coastal region with grid spacing as small as 20 m and its small tributaries with that at less than 10 m, and it provides a first complete list of top potential sites for tidal power generation at NJ coast.

It is anticipated that the identified sites and estimates of their associated parameters will be applicable to actual development of tidal power, and the research of this paper provides a platform for growth of renewable energy industry in the NJ State and the NY State. Once some sites are selected from the lists identified in this research, field measurement is recommended to further validate and characterize the flows. In addition, a 3D simulation could provide more accurate information of tidal power at the selected sites [62,63]. Moreover, a computation of tidal flow using an integration of a model for local 3D flows at power generation facilities with another model for background tidal flows, such as those in [28], will be a substantial progress since it will provide an unprecedented accuracy and detail for flows at local sites. It is worthy of studying these topics in the future.

References

- [1] International Energy Agency. World Energy Outlook 2007; 2007.
- [2] Taylor, FW, The greenhouse-effect and climate change. Reports on Progress in Physics 1991; 54:881-918.

- [3] Tang HS, Chien S. I-Jy, Temimi M, Blain CA, Qu K, Zhao LH, Kraatz S. Vulnerability of population and transportation infrastructure at the east bank of Delaware Bay due to coastal flooding in sea-level rise conditions. *Natural Hazards* 2013; 69:141-163.
- [4] Craft C, Clough J, Ehman J, Joye S, Park R, Pennings S, Guo H, Machmuller M, Forecasting the effects of accelerated sea-level rise on tidal marsh ecosystem services Source: *Frontiers in Ecology and the Environment* 2009; 7:73-78.
- [5] Almas A-J, Hygen HO, Impacts of sea level rise towards 2100 on buildings in Norway. *Building Research & Information* 2012; 40:245-259.
- [6] BP, BP statistical review of world energy, 2008.
- [7] Carley, S. State renewable energy electricity policies: An empirical evaluation of effectiveness. *Energy Policy* 2009; 37:3071–3081.
- [8] Haas R, Panzer C, Resch G, Ragwitz M, Reece G, Held A. A historical review of promotion strategies for electricity from renewable energy sources in EU countries. *Renewable & Sustainable Energy Reviews* 2011;15(2):1003-1034.
- [9] Esteban, M, Leary, D. Current developments and future prospects of offshore wind and ocean energy. *Applied Energy* 2012;90(1):128-136.
- [10] Liu HW, Ma S, Li W, Gu HG, Lin YG, Sun XJ. A review on the development of tidal current energy in China. *Renewable & Sustainable Energy Reviews* 2011; 15(2):1141-1146.
- [11] UK Dept. of Trade and Industry. Energy white paper: our energy future-creating a low carbon economy. Department of Trade and Industry, London, 2003.
- [12] Copping AE, Geerlofs SH. Marine and hydrokinetic energy development technical Support and general environmental studies. PNNL-19081. 2010.
- [13] Polagye B, Cleve BV, Copping A, Kirkendall K, ed. Environmental effects of tidal energy development. Proceedings of a Scientific Workshop March 22-25, 2010. U.S. Dept. of Commerce. NOAA Nat. Marine Fisheries Service.
- [14] Verdant Power. <http://verdantpower.com/>.
- [15] NJDOT. Potential tidal power for New Jersey. Bureau of Research, New Jersey Department of Transportation, Program Project 2010-15, 2010.
- [16] O'Rourke, F, Boyle, F, Reynolds, A. Tidal current energy resource assessment in Ireland: Current status and future update. *Renewable & Sustainable Energy Reviews* 2010;14(9): 3206-3212.
- [17] Evans, P, Armstrong, S, Wilson, C, Fairley, I, Wooldridge, C, Masters, I. Characterisation of a highly energetic tidal energy site with specific reference to hydrodynamics and bathymetry. <http://www.academia.edu/4237228/>
- [18] Energy Technologies Institute. Modelling tidal energy resources. Oct. 18, 2011. http://www.eti.co.uk/news/article/modelling_tidal_energy_resources
- [19] Grabbe, M, Lalander, E, Lundin, S, Leijon, M. A review of the tidal current energy resource in Norway. *Renewable and Sustainable Energy Reviews* 2009; 13:1898–1909

- [20] Defne Z, Haas KA, Fritz HM, Jiang LD, French SP, Shi X, Smith BT, Neary VS, Stewart KM. National geodatabase of tidal stream power resource in USA. *Renewable & Sustainable Energy Reviews* 2012; 16(5):3326-3338.
- [21] USDOE, Energy Efficiency and Renewable Energy Golden Field Office, Marine and hydrokinetic (wave) testing infrastructure development, Funding opportunity announcement Number: DE-FOA-0000847, 07/03/2013.
- [22] Blunden, LS, Bahaj, AS, Aziz, NS. Tidal current power for Indonesia? An initial resource estimation for the Alas Strait. *Renewable Energy* 2013; 49:137-142
- [23] Chen, W-B, Liu, W-C, Hsu, M-H. Modeling assessment of tidal current energy at Kinmen Island, Taiwan. *Renewable Energy* 2013; 50:1073-1082.
- [24] Vennell, R. Estimating the power potential of tidal currents and the impact of power extraction on flow speeds. *Renewable Energy* 2011; 36:3558-3565.
- [25] Carballo R, Iglesias, G Castro A. Numerical model evaluation of tidal stream energy resources in the Ri´a de Muros (NW Spain), *Renewable Energy* 2009; 34:1517–1524
- [26] Xia J, Falconer RA, Lin B. Numerical model assessment of tidal stream energy resources in the Severn Estuary, UK. <http://www.academia.edu/1187905/>
- [27] Walters, RA, Tarbotton, MR, Hiles, CE. Estimation of tidal power potential. *Renewable Energy* 2013; 51:255-262
- [28] Work, PA, Haas, KA, Defne, Z, Gay, T. Tidal stream energy site assessment via three-dimensional model and measurements. *Applied Energy* 2013;102(SI):510-519.
- [29] Tang HS, Kraatz S, Qu K, Chen GQ, Aboobaker N, and Jiang CB. High-resolution survey for tidal energy and influence of sea-level-rise: a case study at coast of New Jersey, USA. *Renewable & Sustainable Energy Reviews* 2014; 32:960–982.
- [30] Bason R, Carnahan S, Makofka N. Developing a New Jersey statewide tidal energy system: preliminary assessment of sites and factors. Project Report 140-02, Natural Currents Energy Services, LLC, 2011
- [31] Advameg, Inc. New Jersey - Location, size, and extent. <http://www.city-data.com/states/New-Jersey-Location-size-and-extent.html>, 2010.
- [32] NOAA national geophysical data center. <http://www.ngdc.noaa.gov/>.
- [33] Edwards M. Global gridded elevation and bathymetry on 5-minute geographic grid (ETOPO5). NOAA, National Geophysical Data Center, Boulder, Colorado, USA, 1989.
- [34] Parker B, Milbert D, Hess K, Gill S. National VDatum - The Implementation of a National Vertical Datum Transformation Database. U.S. Hydrographic Conference, Biloxi, Mississippi, March 24-27, 2003.
- [35] NOAA Coastal Services Center. NOAA composite coastline. <http://shoreline.noaa.gov/data/datasheets/composite.html>.
- [36] NOAA National Geophysical Data Center. Shoreline/Coastline Resources. <http://www.ngdc.noaa.gov/mgg/shorelines/shorelines.html>.
- [37] USGS. USGS water data for the nation. <http://waterdata.usgs.gov>.
- [38] NJ Coastal Planning Areas http://www.state.nj.us/dep/gis/digidownload/images/statewide/coast_pa.gif

- [39] Peltier W, Global glacial isostatic adjustment and modern instrumental records of relative sea level history. *International Geophysics* 2001;75:65–95.
- [40] Yin J, Schlesinger ME, Stouffer RJ. Model projections of rapid sea-level rise on the northeast coast of the United States. *Nature Geoscience* 2009;2:262 – 266.
- [41] Solomon S, Qin D, Manning M, Alley RB, Berntsen T, Bindoff NL, Chen Z, Chidthaisong A, Gregory JM, Hegerl GC, Heimann M, Hewitson B, Hoskins BJ, Joos F, Jouzel J, Kattsov V, Lohmann U, Matsuno T, Molina M, Nicholls N, Overpeck J, Raga G, Ramaswamy V, Ren J, Rusticucci M, Somerville R, Stocker TF, Whetton P, Wood RA, Wratt D, 2007: Technical Summary. In: *Climate Change 2007: The Physical Science Basis. Contribution of Working Group I to the Fourth Assessment Report of the Intergovernmental Panel on Climate Change* [Solomon S, Qin D, Manning M, Chen Z, Marquis M, Averyt KB, Tignor M, Miller HL. (eds.)]. Cambridge University Press, Cambridge, United Kingdom and New York, NY, USA.
- [42] Pfeffer WT, Harper JT, O’Neel SO. Kinematic constraints on glacier contributions to 21st century sea-level rise. *Science* 2008;321(5894):1340–1343.
- [43] Chen C, Liu H, Beardsley RC. An unstructured grid, finite-volume, three-dimensional, primitive equations ocean model: Application to coastal ocean and estuaries. *Journal of Atmospheric and Oceanic Technology* 2003;20:159–186.
- [44] Egbert G, Bennett A, Foreman M. Topex/poseidon tides estimated using a global inverse model. *Journal of Geophysical Research* 1994;24:821–852.
- [45] NOAA National Buoy Data Center. <http://www.ndbc.noaa.gov/>.
- [46] Chen C, Beardsley RC, Cowles G. FVCOM User Manual. 2nd edition, 2006.
- [47] Peixoto JP, Oort AH. *Physics of Climate*, Springer-Verlag New York, Inc., 1992.
- [48] CUNY High Performance Computing Center.
http://www.csi.cuny.edu/cunyhpc/HPC_Systems.html .
- [49] The National Energy Research Scientific Computing Center <http://www.nersc.gov/about/>.
- [50] Urban Ocean Observatory at Davidson Laboratory. New York harbor observing and prediction system. <http://hudson.dl.stevens-tech.edu/maritimeforecast/>.
- [51] Kraatz S. High-resolution numerical simulation of tidal energy distribution along the New Jersey coastline and influence of sea-level rise. MS thesis. Dept. Civil Eng., City Collge of New York. 2012.
- [52] Tang HS, Sotiropoulos F, Fractional step artificial compressibility method for Navier-Stokes equations, *Computers & Fluids* 2007; 36:974-986.
- [53] Defne Z, Haas KA, Fritz HM. Numerical modeling of tidal currents and the effects of power extraction on estuarine hydrodynamics along the Georgia coast, USA. *Renewable Energy* 2011; 36:3461-3471.
- [54] Khan MJ, Bhuyan G, Iqbal MT, Quaicoe JE. Hydrokinetic energy conversion systems and assessment of horizontal and vertical axis turbines for river and tidal applications: A technology status review. *Applied Energy* 2009;86:1823–1835.

- [55] Tang HS, Skraatz S, Performance Indicators for marine hydrokinetic energy generation systems. Proc. ASCE 2011 Structures Congress, D. Ames, T. L. Droessler, and M. Hoit (Ed.), 1236-1245.
- [56] Bedard R, Previsic M, Siddiqui O, Hagerman G, Robinson M. North American Tidal In Stream Energy Conversion Feasibility Demonstration Project. EPRI TP-04-NA. Electric Power Research Institute; 2006.
- [57] Myers L, Bahaj AS. Simulated electrical power potential harnessed by marine current turbine arrays in the Alderney Race. *Renewable Energy* 2005;30:1713–31.
- [58] Defne Z, Haas KA, Fritz M. GIS based multi-criteria assessment of tidal stream power potential: A case study for Georgia, USA. *Renewable & Sustainable Energy Reviews* 2011; 15(5):2310-2321.
- [59] Thomas K, Grabbe M, Yuen K, Leijon M. A low speed generator for the energy conversion from marine currents -- experimental validation of a simulation. *Proceedings of the IMechE Part A: Journal of Power and Energy* 2008; 222:381-388
- [60] Vermaak HJ, Kusakana K, Koko SLP. Status of micro-hydrokinetic river technology in rural applications: A review of literature. *Renewable & Sustainable Energy Reviews* 2014; 29:625-633
- [61] Gunawan B, Neary VS and Colby J. Mean velocity and turbulence measurements at a tidal energy site in East River, NY (USA). *Renewable Energy*, accepted.
- [62] Tang HS, Wu XG. CFD and GFD hybrid approach for simulation of multi-scale coastal ocean flow. *Modelling for Environment's Sake, Fifth Biennial Meeting, Ottawa, Canada.* Swayne DA, Yang WH, Voinov AA, Rizzoli A, Filatova T. (Eds.). 2010.
- [63] Tang HS, Qu K, Wu XG. An overset grid method for integration of fully 3D fluid dynamics and geophysics fluid dynamics models to simulate multiphysics coastal ocean flows. *J. Comput. Phys.*, 2013, submitted.

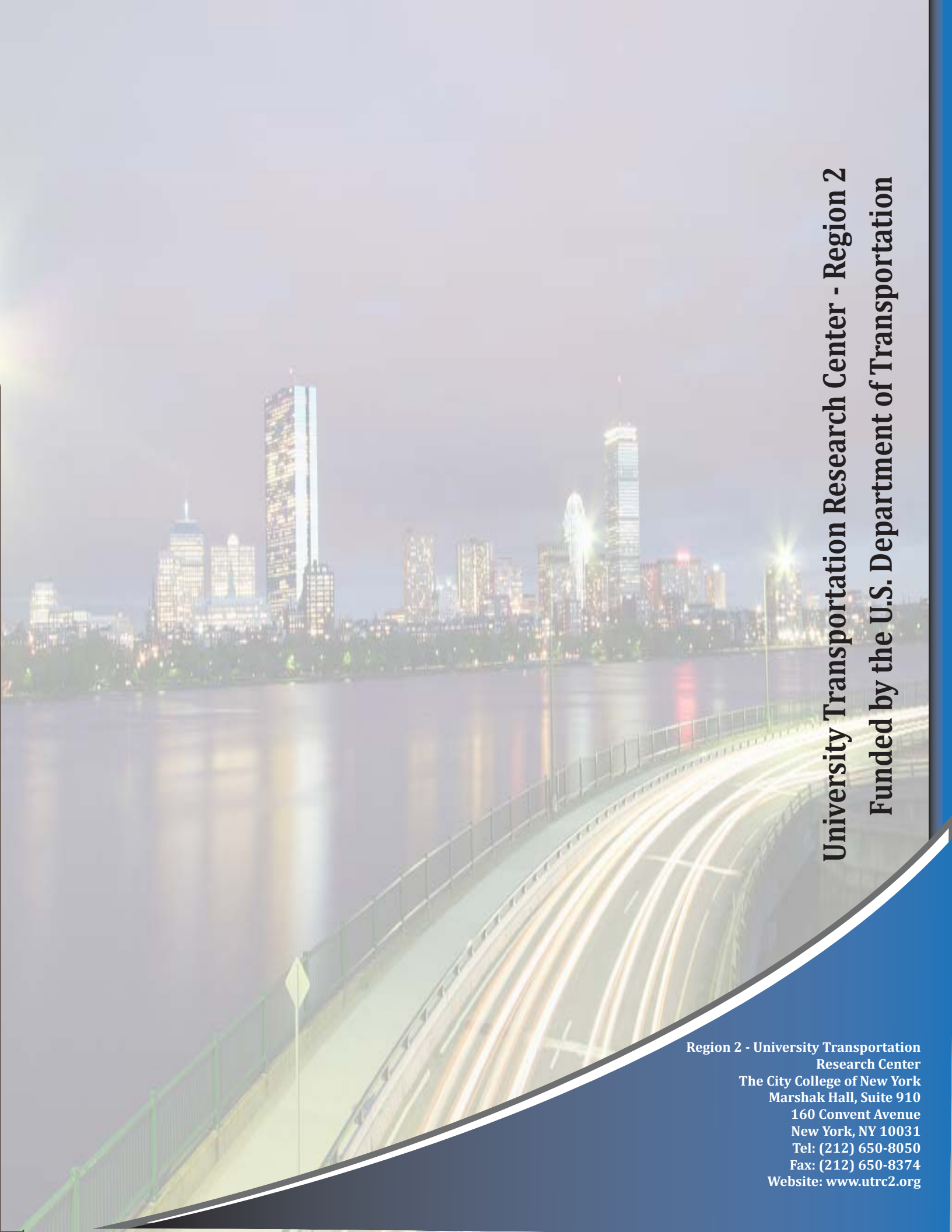
Appendix A: Observation stations

The names and locations of the 47 coastal observation stations used in calibration of the model are as follows [37,45,50].

Station	Name	Lon.	Lat.	Station	Name	Lon.	Lat.
1	New London	-72.090	41.360	25	Little Egg	-74.325	39.509
2	Montauk	-71.960	41.048	26	Absecon Cr.	-74.484	39.415
3	New Haven	-72.911	41.275	27	Atlantic City	-74.418	39.355
4	Bridgeport	-73.173	41.155	28	Route 40	-74.456	39.353
5	King's Point	-73.766	40.810	29	Margate	-74.513	39.337
6	Point Lookout	-73.580	40.564	30	Ingram Thorof.	-74.734	39.110

7	G.W.Bridge	-73.950	40.850
8	Battery	-74.011	40.699
9	Bergen	-74.142	40.640
10	Narrows	-74.039	40.608
11	South Amboy	-74.281	40.492
12	Keansburg	-74.148	40.450
13	Belford	-74.081	40.436
14	Sandy Hook	-74.017	40.463
15	Navesink Riv.	-74.014	40.382
16	Shrewsbury Riv.	-73.975	40.366
17	Branchport Cr.	-73.997	40.323
18	Shark Riv.	-74.030	40.181
19	Point Pleasant	-74.038	40.102
20	Mantoloking	-74.052	40.040
21	Seaside Heights	-74.082	39.938
22	Barnegat Light	-74.109	39.763
23	Waretown	-74.182	39.781
24	Ship Bottom	-74.186	39.654

31	Stone Harbor	-74.764	39.057
32	Cape May Harb.	-74.891	38.949
33	Brown Shoal Lt.	-75.012	38.921
34	Lewes	-75.116	38.810
35	Cape May	-74.960	38.968
36	Brandywine Shl	-75.113	38.987
37	South Dennis	-74.888	39.158
38	Maurice River	-75.033	39.232
39	Ship John Shoal	-75.375	39.305
40	Reedy Point	-75.573	39.558
41	Delaware City	-75.590	39.582
42	Marcus Hook	-75.410	39.812
43	Philadelphia	-75.142	39.933
44	Tacony-Palmyra	-75.042	40.012
45	Burlington	-74.872	40.080
46	Kiptopeke	-75.988	37.165
47	Cape Henry	-76.013	36.960

A long-exposure photograph of a city skyline at night, reflected in a body of water. In the foreground, a bridge or highway is visible with light trails from moving vehicles. The sky is dark, and the city lights are bright and colorful.

University Transportation Research Center - Region 2
Funded by the U.S. Department of Transportation

**Region 2 - University Transportation
Research Center**
The City College of New York
Marshak Hall, Suite 910
160 Convent Avenue
New York, NY 10031
Tel: (212) 650-8050
Fax: (212) 650-8374
Website: www.utrc2.org